Contributions of U-Th-Pb dating on the diagenesis and sediment sources of the lower group (BI) of the Mbuji-Mayi Supergroup (Democratic Republic of Congo)

C. François, B.K. Baludikay, J.Y. Storme, D. Baudet, Jean-Louis Paquette, M. Fialin, E.J. Javaux

CrossMark

Contributions of U-Th-Pb dating on the diagenesis and sediment sources of the lower group (BI) of the Mbuji-Mayi Supergroup (Democratic Republic of Congo)

C. François [a],[*], B.K. Baludikay [a], J.Y. Storme [a], D. Baudet [b], J.L. Paquette [c], M. Fialin [d], E.J. Javaux [a]

[a] Paleobiogeology-Paleobotany-Paleopalynology Lab, Department of Geology, UR Geology, B18, University of Liege, 4000 Liège, Belgium
[b] Geodynamics and Mineral Resources Service, Royal Museum for Central Africa, Tervuren, Belgium
[c] Laboratoire Magmas & Volcans, Université Clermont Auvergne, CNRS-IRD-OPGC, 63000 Clermont-Ferrand, France
[d] Camparis, Université Paris 6, 4 Place Jussieu, 75252 Paris Cedex 5, France

ARTICLE INFO

ABSTRACT

In this paper, we present new age constraints for the lower part of the Meso-Neoproterozoic sedimentary Mbuji-Mayi Supergroup (Democratic Republic of Congo, DRC). This Supergroup preserves a large diversity of organic-walled microfossils, evidencing the diversification of early eukaryotes for the first time in Central Africa. We use different methods such as *in situ* U-Pb geochronology by LA-ICP-MS and U-Th-Pb chemical datings by Electron Microprobe on diagenetic and detrital minerals such as xenotimes, monazites and zircons. We attempt to better constrain the provenance of the Mbuji-Mayi sediments and the minimum age of the Mbuji-Mayi Supergroup to constrain the age of the microfossils. Results with LA-ICP-MS and EMP provide new ages between 1030 and 1065 Ma for the diagenesis of the lower part of the sedimentary sequence. These results are consistent with data on biostratigraphy supporting the occurrence of worldwide changes at the Mesoproterozoic/Neoproterozoic boundary.

© 2017 The Authors. Published by Elsevier B.V. This is an open access article under the CC BY-NC-ND license (http://creativecommons.org/licenses/by-nc-nd/4.0/).

1. Introduction

The Mbuji-Mayi Supergroup (former "Système de la Bushimay"), DRC, (Figs. 12) located between the Archean-Paleoproterozoic Congo-Kasai Craton and the Mesoproterozoic Kibara Belt, consists of a sedimentary sequence unaffected by regional metamorphism during this long history (Raucq, 1957, 1970; Baludikay et al., 2016b). Recently, a large diversity of well-preserved acritarchs (organic-walled microfossils) was described including a total of 49 taxa belonging to 27 genera (Baludikay et al., 2016a). This microfossil assemblage comprises 11 species of unambiguous eukaryotes, 10 species of possible eukaryotes or prokaryotes and 28 species of probable bacteria, attesting for the first time the diversification of complex life (early eukaryotes) in Meso/Neoproterozoic redox stratified oceans of Central Africa. The Mbuji-Mayi Supergroup did not suffer high metamorphism and deformation due to its location within the broad Congo-Kasai Craton, away from the Pan-African orogeny that developed at its margin during the final amalgamation of Gondwana. These favorable conditions permitted a good preservation of the micro-

fossils and also of the diagenetic minerals. Dating this Supergroup has been and is still a challenge despite several attempts. Recently, Delpomdor et al. (2013) provided a maximum age for the lower part of the Supergroup (BI Group) only based on detrital zircon ages. In this study, we combine different geochronological methods, in particular on diagenetic minerals such as monazite and xenotime but also on detrital zircons. Our new results permit to provide better constraints on the age of the Mbuji-Mayi Supergroup, on the complex timing and source of sediments filling the basin, of its microfossil assemblage, and importantly, on the diversification of early eukaryotes in central Africa.

2. Geological setting of Mbuji-Mayi Supergroup

The Mbuji-Mayi Supergroup is located in the Sankuru-Mbuji-Mayi-Lomami-Lovoy (SMLL) basin (Fig. 1), an intracratonic failed-rift basin (Kadima et al., 2011) located at the northern part of the Congo-Kasai Craton (DRC) between 5°S and 9°S and 23°E and 26°E. This Archean/Paleoproterozoic craton was edged by the Kibara (1.4–1.0 Ga, in the northeast) and Irumide (ca. 1.02 Ga, in the southeast) orogenic belts (Johnson et al., 2005; De Waele and Fitzsimons, 2007; De Waele et al., 2008; Begg et al., 2009; Fernandez-Alonso et al., 2012). In this paper, we focused our work

* Corresponding author.
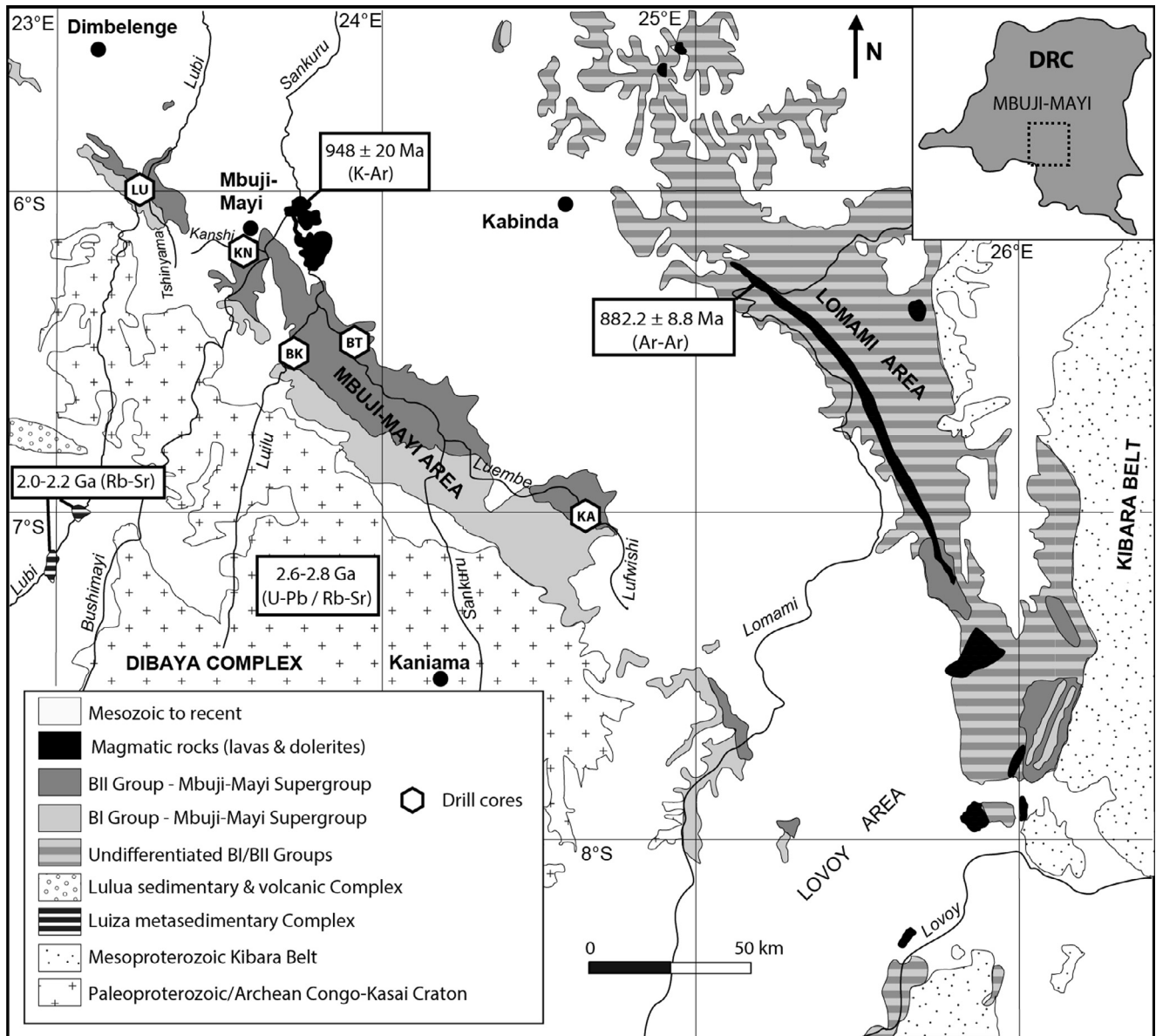   E-mail address: c.francois@ulg.ac.be (C. François).

Fig. 1. Geological map of the Sankuru-Mbuji-Mayi-Lomami-Lovoy (SMLL) basin. Drill cores: LU: Lubi, KN: Kanshi, BK: Bena Kalenda, BT: Bena Tshovu and Ka: Kafuku. Age data from Cahen et al. (1954, 1972, 1984), Cahen (1974), Holmes and Cahen (1955) and Delpomdor et al. (2013). Map modified after Delpomdor et al. (2013).

in the western part of the SMLL basin between the Dibaya Complex to the south (2.6–2.8 Ga; Delhal et al., 1975; Cahen et al., 1984; Delpomdor et al., 2013), corresponding to the northern part of the Congo-Kasai Craton, and the Mesoproterozoic Kibara Belt to the east.

Cores were drilled during the 1950s in the Sankuru-Mbuji-Mayi area, in several locations between the Lubi (East Kasai) and Luembe rivers (North Katanga; Figs. 1 and 2) and are stored today in the collections of the Royal Museum for Central Africa (RMCA) in Tervuren (Belgium). Detailed petrological descriptions of these drill cores were carried out by Wazilewski (1953) and Raucq (1957, 1970), which allowed recognition of corresponding stratigraphic units. Delpomdor (2013) updated these descriptions using a newer sedimentological model.

The lithostratigraphy of the Supergroup consists of two Groups (Fig. 2). The lower siliciclastic sequence (BI Group; ~500 m thick) is poorly age-constrained and approximatively dated between ca.

1174 ± 22 Ma (Delpomdor et al., 2013) and ca. 1055 Ma (Cahen, 1954; Holmes and Cahen, 1955; Raucq, 1957; Cahen, 1974). It is unconformably overlying the ca. 2.8–2.6 Ga granitoid Dibaya Complex (Delhal et al., 1975; Cahen et al., 1984; Delpomdor et al., 2013). The upper carbonated sequence (BII Group; ~1000 mthick) is intercalated with sparse organic-rich shales and is partially covered by lavas dated around 950 Ma (Cahen et al., 1974, 1984).

The sedimentary sequence is unaffected by regional metamorphism, temperatures recorded by the basin are lower than 300 °C (Raucq, 1957, 1970; Baludikay et al., 2016b). Siliciclastic sequences (BI Group) are found in particular, in the S70 Tshinyama drill core (named hereafter "Lubi"; samples RG57624 to 57826 of the RMCA serial number collection) and Kafuku 15 drill core (named hereafter "Kafuku"; samples RG41330–41384). The BI Group consists of six Subgroups: BIa, BIb, BIc, BId, BIE and BIe. This Group is mostly siliciclastic, and starts with deposition
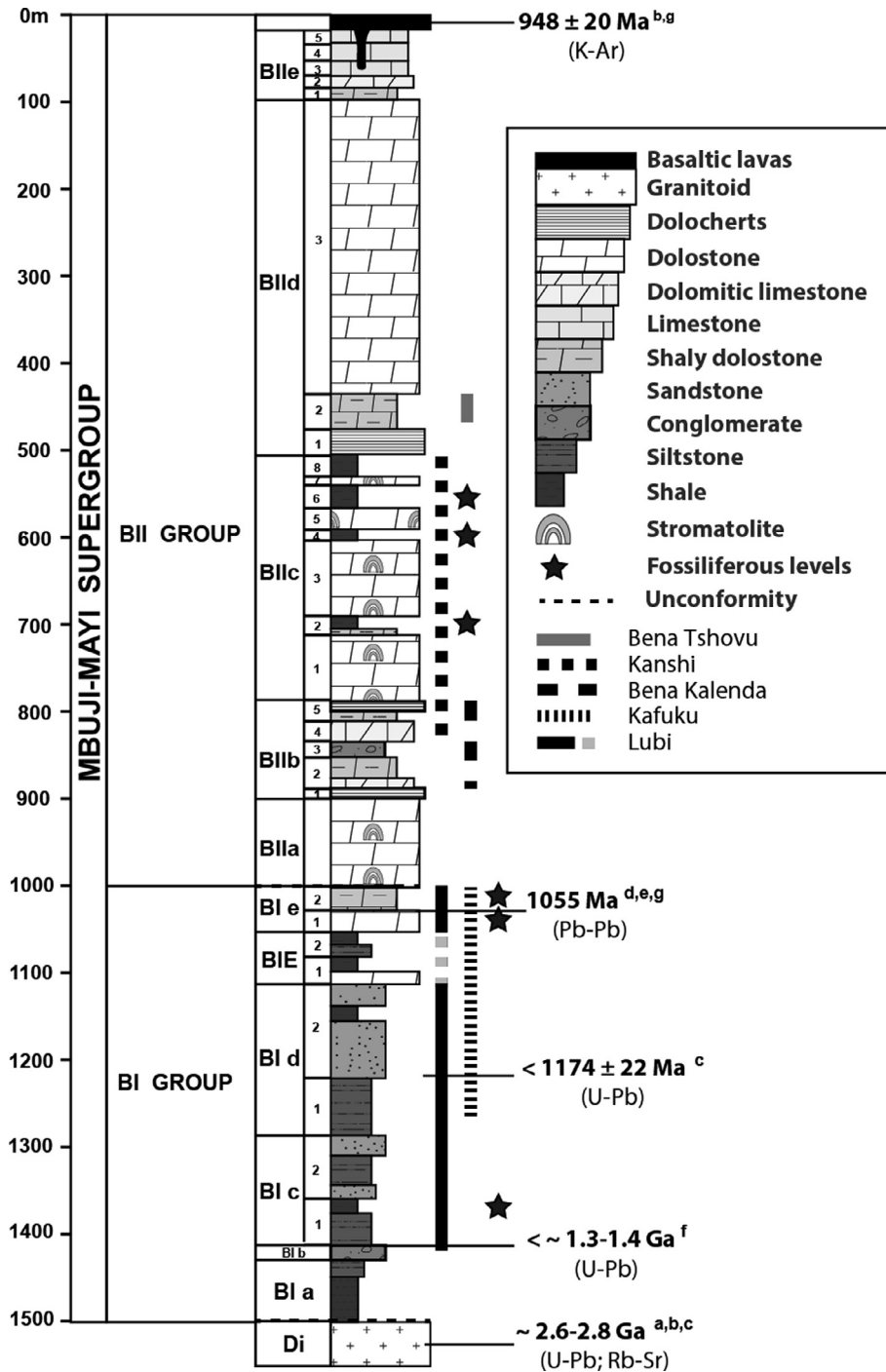
Fig. 2. Stratigraphy of the Mbuji-Mayi area. Ages from (a) Delhal et al. (1975), (b) Cahen et al. (1984), (c) Delpomdor et al. (2013), (d) Cahen (1954), (e) Holmes and Cahen (1955), (f) Cahen (1972) and (g) Cahen (1974). Log modified from Raucq (1957, 1970) and Baludikay et al. (2016a).

in shallow water, with signs of emersion observed in the Lubi drill core (mudcracks and gypsum). Carbonated sequences (BII Group) are found in the Bena-Kalenda drill core, Kanshi S13B drill core (named hereafter "Kanshi"; samples RG32201 to RG32464), as well as Bena-Tshovu drill core (samples RG31534–RG31646). The BII Group, including mainly transgressive carbonates, consists of five Subgroups: BIIa, BIIb, BIIc, BIId and BIIe. Detailed descriptions of these Subgroups have been given in Raucq (1957, 1970) and were updated (especially for

the carbonates) by Delpomdor (2013) and Delpomdor et al. (2015). The BII Group is alternately marked by the development of stromatolites interbedded with thin detrital levels or by thick layers of carbonates with cherts, corresponding to a long subsidence regime without terrigenous contributions (Bertrand-Sarfati, 1972). The regular intraformational breccias or conglomerates throughout the BII (b, c, and e) Group reflect the instability of the basin and its tendency of emersion in oxidizing environment (Delhal and Ladmirant, 1979).

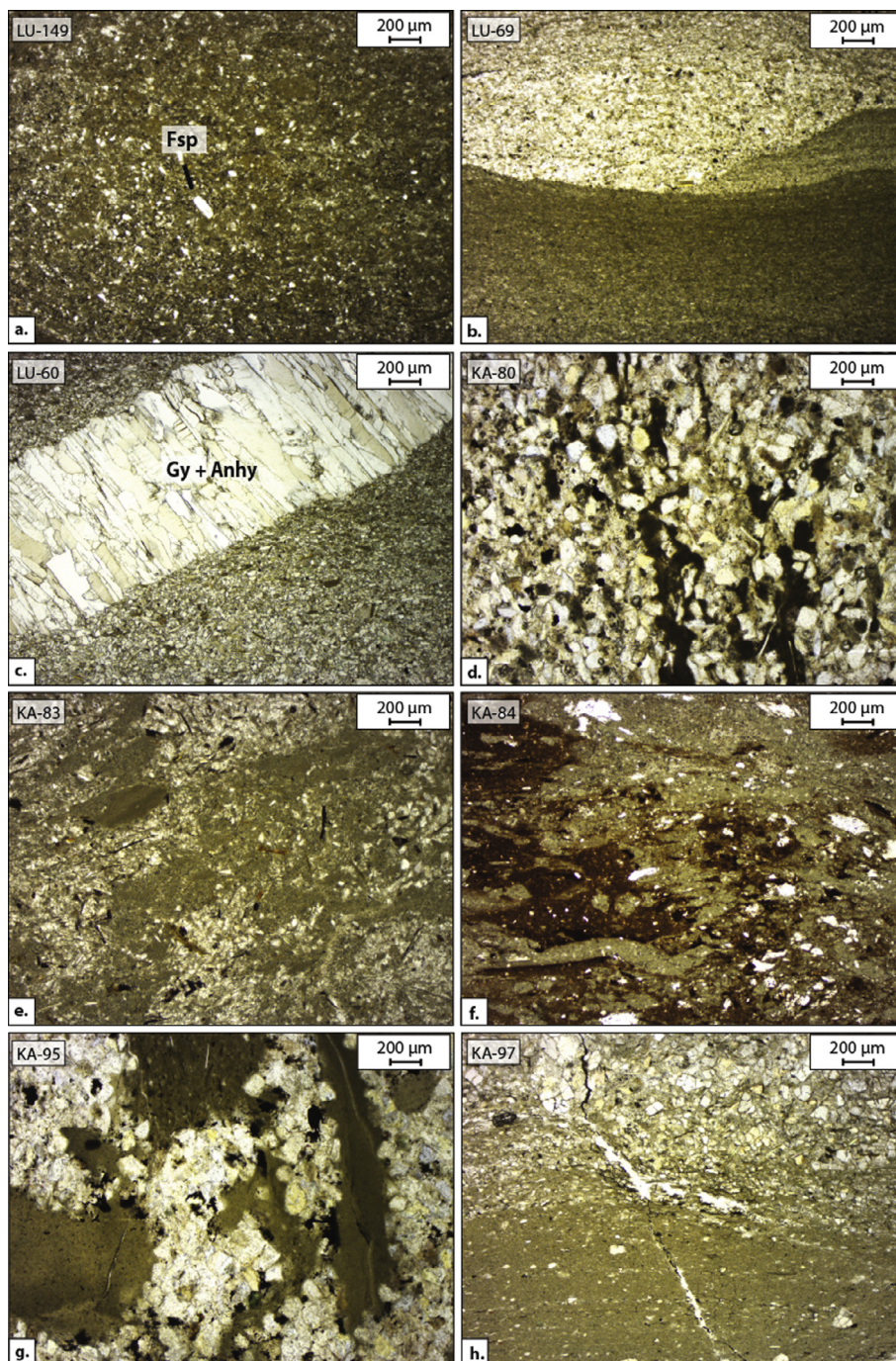**Fig. 3.** Photomicrographs of (a) sample LU-149: siltstone with feldspar, quartz and white mica, (b) sample LU-69: mudstone with feldspar, quartz, biotite, chlorite, white mica, apatite and barite, (c) sample LU-60: siltstone composed of quartz, feldspar, white mica, biotite and chlorite with large fractures of gypsum, anhydrite and celestite, (d) sample KA-80: sandstone showing flakes of clay minerals in a matrix of quartz, feldspar and white micas, (e) sample KA-83: argillaceous siltstone with quartz, feldspar, carbonate, biotite, chlorite and oxide, (f) sample KA-84: shaly dolomite with feldspar, quartz and dolomite megacrysts, (g) sample KA-95: carbonated argillaceous sandstone with quartz, mica, oxide, clay and carbonate and (h) sample KA-97: micaceous sandstones with feldspar, quartz, biotite, chlorite and oxide.

Basaltic lavas topping the Mbuji-Mayi Supergroup in the northeast of the Mbuji-Mayi area (Figs. 1 and 2) were dated at 948 ± 20 Ma (Cahen et al., 1974, 1984). The emplacement of these summital basalts marked the end of the sedimentary sequence.

3. Previous geochronological studies

The Mbuji-Mayi Supergroup unconformably overlies the ca. 2.9–2.6 Ga granitoid Dibaya Complex (Figs. 1 and 2). This age was obtained by Rb-Sr method (whole rock) on migmatites and granites (2648 ± 22 Ma and 2593 ± 92 Ma; Delhal et al., 1975; Cahen et al., 1984) and by U-Pb dating (ca. 2680 Ma on zircons, monazites and titanites; Delhal et al., 1975; Cahen et al., 1984 and around 2.8–2.7 Ga on zircons; Delpomdor et al., 2013).

A thermo-tectonic event was dated at ca. 2000–2200 Ma (Cahen et al., 1984) by Rb-Sr method on muscovite from micaschistes of the Luiza metasedimentary Complex (Fig. 1; Delhal and Ladmirant, 1979). These metasedimentary rocks occur as isolated

patches to the west of 23°E lying unconformably on the Archean to Paleoproterozoic Kanda-Kanda tonalites and granodiorite gneisses.

To the east, the Archean to Paleoproterozoic craton was then marked by the Kibara (1.4–1.0 Ga) orogenic cycle (Fig. 1; Cahen et al., 1984; Johnson et al., 2005; De Waele and Fitzsimons, 2007; de Waele et al., 2008; Begg et al., 2009; Fernandez-Alonso et al., 2012) occurring in Central Africa in Mesoproterozoic times during convergence between the Tanzania-Bangweulu Craton and the Congo-Kasai Craton. A plutonic activity is recorded around 1.3–1.4 Ga, poorly dated first between 1310 and 1350 Ma (Cahen et al., 1974). More recent compilations (Tack et al., 2002; Kokonyangi et al., 2004; Tack et al., 2010) restrict the Kibara tectono-magmatic event around 1.37–1.38 Ga (samples from the Kibara hills type-locality close to Mitwaba town).

U-Pb ages on detrital zircons obtained directly on sediments from the Mbuji-Mayi Supergroup, were analyzed by Delpomdor et al. (2013). The youngest concordant grain is dated at 1174 ± 22 Ma (BId2 Formation in Kafuku drill core) and thus gives a maximum age around 1175 Ma for the sedimentation of the BI Group (Fig. 2).

Three samples of galena, from the Lubi and Senga-Senga valleys and from the contact between BIIa and BIIb in Luembe valley (namely Kafuku) yielded conventional $^{207}Pb/^{206}Pb$ ages of 910 Ma, 1040 Ma and 1065 Ma (Cahen, 1954; Holmes and Cahen, 1955; Raucq, 1957). Ages of 1040 and 1065 Ma have been attributed to syngenetic growth of galena and provide an age around 1055 Ma for the top of BI Group (BIe; Cahen, 1974; Fig. 2).

Basaltic lavas topping the BII group at the confluence of the Mbuji-Mayi and Sankuru Rivers provided five nearly concordant K-Ar whole rock ages (Cahen et al., 1974, 1984; Figs. 1 and 2) ranging from 870 ± 20 Ma to 953 ± 20 Ma. Among these, three results obtained on two samples were concordant: 916 ± 20 Ma, 942 ± 20 Ma, and 953 ± 20 Ma. An estimated age of 948 ± 20 Ma has been retained, corresponding to the two older ages. Note that the authors indicated that analyzes were carried out on altered samples and that no geochemical controls were used in the sample selection.

Moreover, studies of Mbuji-Mayi stromatolites by Bertrand-Sarfati (1972) compared to series in Mauritania suggested the deposition of the BII Group between around 1020 Ma and 910 Ma (isochrones by Bonhomme and Clauer, 1972; Clauer, 1973).

In the Lomami area (eastern part of the SMLL basin) an Ar-Ar dating on whole rock samples of dolerite sills gave an age of 882.2 ± 8.8 Ma (Delpomdor et al., 2013). These dolerites were interpreted as emplaced close to the contact between the BI and BII Groups and were attributed to the BI/BII limit by Cahen et al. (1984) and Delpomdor et al. (2013, 2015). However, in the Lomami area, BI and BII were poorly studied (Fig. 1) and no correlation with the Mbuji-Mayi area can be made. Thus, the stratigraphic position of these Lomami sills need to be confirmed in the field. They were not considered here since they are not directly related to our study.

4. Sample description

To select appropriate lithologies, we observed and sampled the drill cores and also used the lithological descriptions of Raucq (1957, 1970) updated by Delpomdor (2013) and Baludikay et al. (2016a). A total of 41 polished thin sections were cut through the five drill cores to study their petrology, microstructures (Fig. 3) and to look for monazites, xenotimes and zircons with an optical microscope and a Scanning Electron Microprobe (Fig. 4). Unfortunately, the BII Group samples contained no monazite nor xenotime. Only a few zircons were found, preventing a good geochronological statistic. In the BI Group samples, monazites,
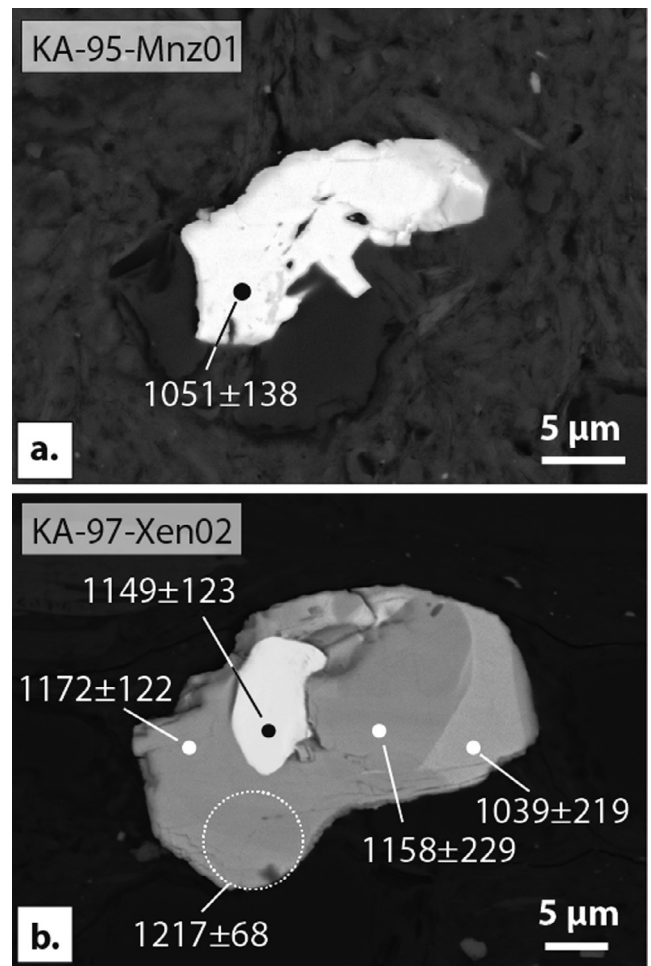
Fig. 4. Backscaterred image for (a) monazite (KA-95) and (b) xenotime with monazite inclusion (KA-97) in Kafuku drill core with location and age of EMP analyzes (errors are 2σ). Dashed white circle in (b) represent size of the LA-ICP-MS $^{207}Pb/^{206}Pb$ spot analysis (error is 2σ).

Table 1
Samples containing monazites, xenotimes or zircons from BI Group used for U-Pb datings.

Sample	Drill core	RG number	Depth	Formation
KA-80	Kafuku	41370	53.25	BIE2
KA-83	Kafuku	41371	62.2	BIE2
KA-84	Kafuku	41371	78.8	BIE1
KA-95	Kafuku	41378	119.25	BId2
KA-97	Kafuku	41384	172.15	BId1
LU-149	Lubi	57661	113.90	BIe1
LU-69	Lubi	57788	257.00	BIc2
LU-60	Lubi	57791	269.00	BIc2

zircons and xenotimes were found in both Lubi and Kafuku drill cores (Table 1).

Samples of the BI Group consist of siliciclastic rocks composed of quartz, carbonates (mainly dolomite, ankerite and siderite), feldspars (K-feldspar and some plagioclase), oxides (anatase, hematite, goethite and lepidocrosite), sulphides (pyrite and marcassite), apatite and some phyllosilicates (white mica, biotite, chlorite and clay; Fig. 3).

In the Lubi drill core, the lithostratigraphic succession (from bottom to top, Delpomdor, 2013) is as follows: BIb Subgroup

Fig. 5. Backscaterred images and X-ray maps (Th Mα, Pb Mβ and U Mβ) for four monazites from Kafuku drill core (a & b) from KA-84 sample and (c & d) from KA-98 sample. Blue spots represent location of EMP analyzes for rims of the different monazites (spots are magnified 6 times for better viewing). Corresponding ages are in tables on the right with corresponding mean age and standard deviation (1σ).

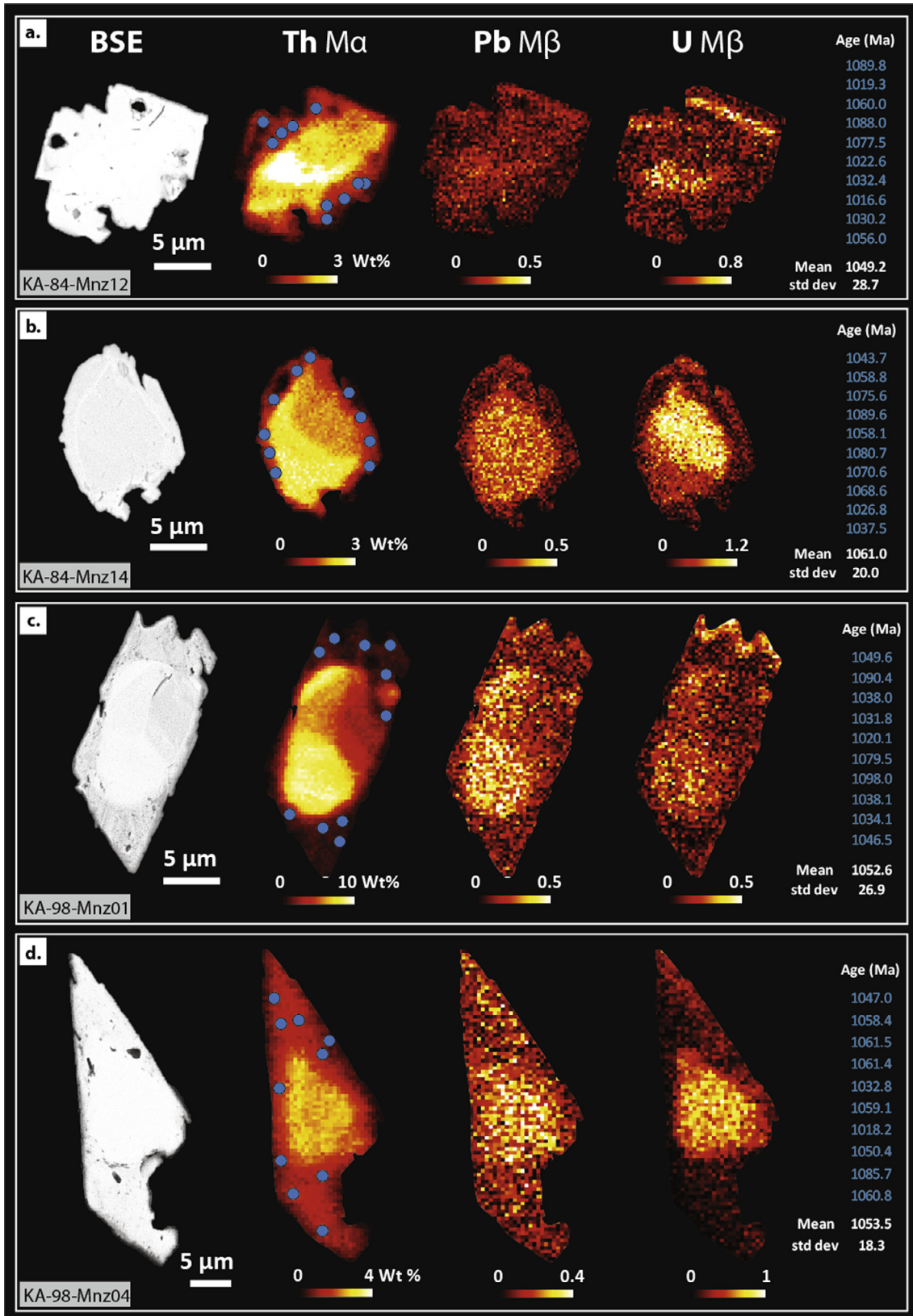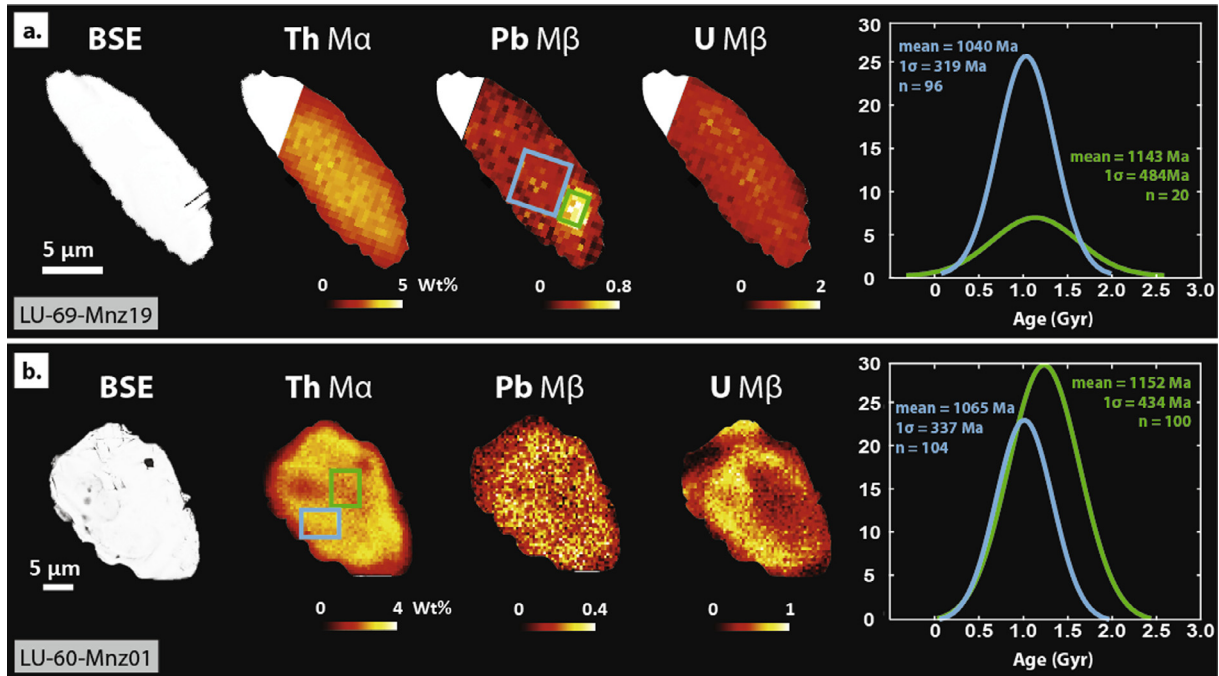**Fig. 6.** Backscaterred images and X-ray maps (Th Mα, Pb Mβ and U Mβ) for two monazites from Lubi drill core and corresponding ages calculated (standard normal distribution of the pixel values from the green and blue areas), showing two distinct age domains, in core (in green) and in rims (in blue) respectively.

consisting of dark conglomeratic sandstones and grey shaly lime-stones covered by alternations of dark micaceous sandstones and grey-pink brecciated dolomitic carbonated argillaceous sand-stones; BIc (130 m) and BId Subgroups (100 m) exhibit micaceous sandstones with quartzites and sandstone in an argillaceous-carbonate matrix (BIc2 Formation, LU-69 & LU-60). Some gypsum and anhydrite veins are also observed in some samples (i.e. LU-60). BIe Subgroup (50 m) is composed of grey shaly dolomites and siltstones (BIe1 Formation, LU-149) below cherty dolomite layers. The uppermost BIe Subgroup (BIe2 Formation, 20 m) con-sists of grey cherty dolomites evolving to grey shaly dolomites and shales.

In the Kafuku drill core, the lithostratigraphic succession (from bottom to top, Delpomdor, 2013) is as follows: BId Subgroup (90 m) composed of pink sandstones and carbonated argillaceous sandstones (BId2 Formation, KA-95) and micaceous feldspathic pink quartzites with bedded micaceous sandstones (BId1 Forma-tion, KA-97); BIE Subgroup (60 m) consists of micaceous shales evolving into argillaceous micaceous sandstones (BIE2 Formation, KA-80, KA-83 & KA-84), argillaceous dolomites and variegated shaly dolomites with gypsum veins, sandy pink and green or varie-gated zoned micaceous sandstones with argillaceous or brecciated dolomites; BIe Subgroup (40 m) exhibits dark argillaceous or silic-eous dolomites with shales and polygenic intraformational breccia, with cherty dolomites passing to dolomitic shaly pink limestones and breccias, micaceous sandstones or carbonated argillaceous sandstones; and the bottom of BIIa Subgroup (10 m) composed of grey stromatolitic dolomites, micaceous pink quartzites and silic-eous dolomites.

The observed xenotimes minerals displayed different mor-phologies: rounded, well crystallized, between grains or in over-growth around zircon (Fig. 7a). Monazites were either rounded, very damaged or small and automorph (Fig. 7b). They occasionally presented zoning. Zircons were very damaged and displayed oscil-latory zoning (Fig. 7c). A total of 37 monazite grains, 10 xenotime grains and 28 zircon grains were selected and dated.

5. Analytical methods

To better constrain the age of the diagenesis through the BI Group of the Mbuji-Mayi Supergroup, our research strategy is focused on different *in situ* technical approaches (i) U-Th-Pb chem-ical dating with Electron MicroProbe on monazites and xenotimes which are inherited and sometimes diagenetic (Montel et al., 1996; McNaughton et al., 1999; Rasmussen and Muhling, 2007) and (ii) U-Pb with Laser Ablation Inductively Coupled Plasma Mass Spec-trometer (LA-ICP-MS) on inherited zircons, xenotimes and monazites.

5.1. U-Th-Pb chemical dating with Electron Microprobe

Electron Microprobe offers a high spatial resolution with a spot less than 1 μm and is a non-destructive method capable to resolve a complex growth history of monazite (Suzuki and Adachi, 1994; Cocherie et al., 1998; Williams et al., 1999; Montel et al., 1996, 2000; Crowley and Ghent, 1999; Terry et al., 2000; Shaw et al., 2001; Williams and Jercinovic, 2002; Goncalves et al., 2004, 2005) but also of xenotime (Suzuki and Adachi, 1991; Griffin et al., 2000; Asami et al., 2002; Harrison et al., 2002). This method also allows for mapping and for a pre-characterization of monazite and xenotime before isotopic analysis. Monazite contains negligible common Pb, only radiogenic Pb (Parrish, 1990), and is a robust geochronometer capable of recording multiple crystallization events including diagenesis in successive zoning around a core.

The theoretical basis for the method consists of measuring U-Th-Pb concentrations in a crystal and of calculating the age (t) by solving the equation:

$$Pb = (Th/232) * [exp(\lambda^{232} * t) - 1] * 208 + (U/238.04) * 0.9928$$
$$* [exp(\lambda^{238} * t) - 1] * 206 + (U/238.04) * 0.0072$$
$$* [exp(\lambda^{235} * t) - 1] * 207$$
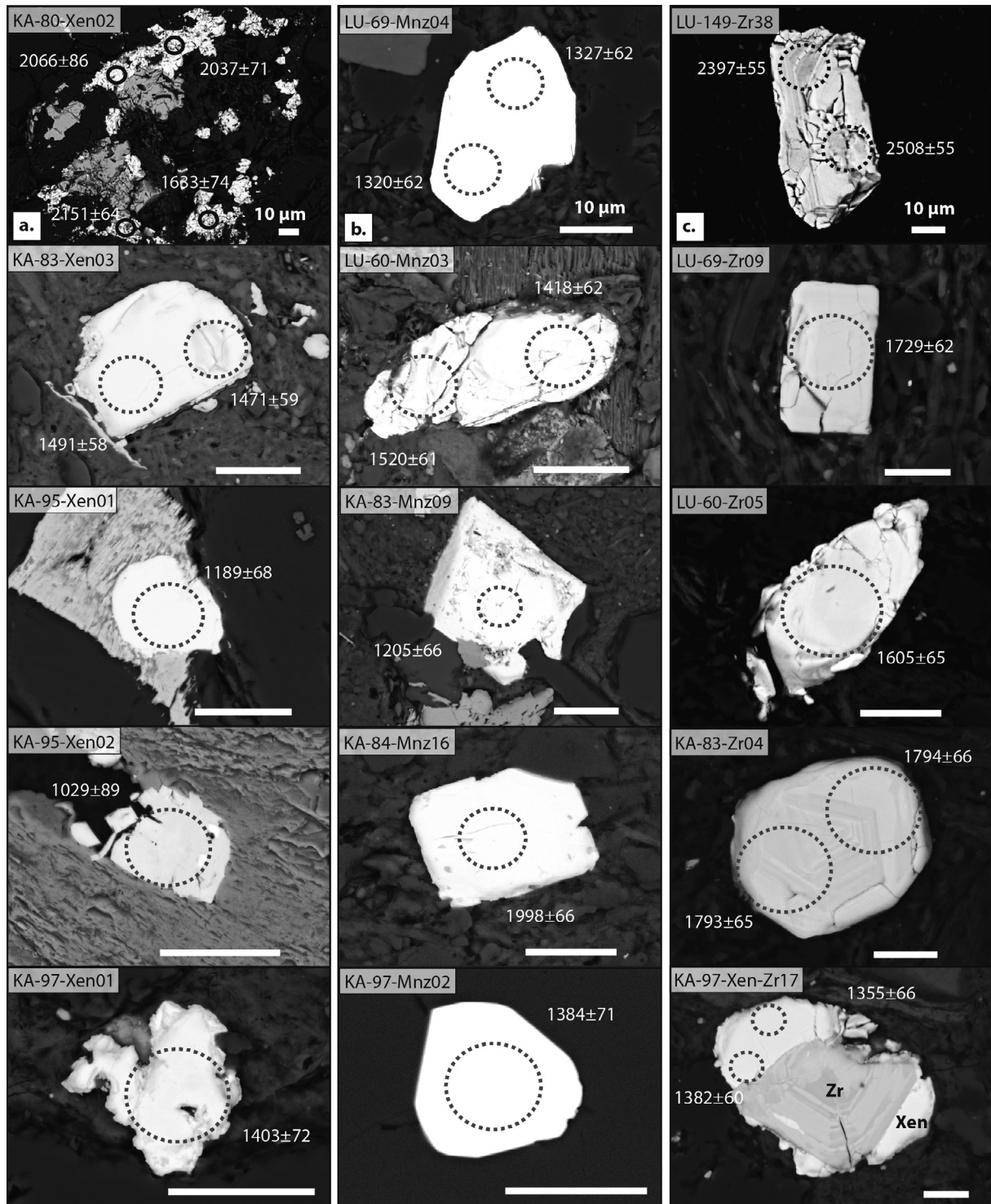
Fig. 7. Backscattered electron imaging of some (a) xenotimes on the left column, (b) monazites on the middle column and (c) zircons on the right column of selected samples from the Kafuku and Lubi drill cores. Circles show location and age (Ma) of LA-ICP-MS ^{207}Pb/^{206}Pb spot analyzes. Scale bar is 10 μm.

where Pb, U, Th are in ppm, and λ^{232}, λ^{235}, λ^{238} are the radioactive decay constants of ^{232}Th, ^{235}U, and ^{238}U, respectively. Because monazite is rich in Th (commonly 3–15 wt%, sometime up to 25%) and U (a few hundreds of ppm up to 5%), radiogenic lead (Pb) accumulates very quickly, and in less than 100 million years reaches a level where a precise measurement can be performed with an Electron Microprobe.

The age calculated by this method has a geological meaning if: (1) non-radiogenic lead is negligible, and (2) no modification of the U/Th/Pb ratios has occurred except by radioactive decay. The validity of these hypotheses, was discussed by Montel et al. (1994; 1996) for monazite and by Suzuki and Adachi (1991), Griffin et al. (2000), Asami et al. (2002) and Harrison et al. (2002) for xenotime.

Table 2
EMP monazite and xenotime analytical data for BI Group. Errors are 2σ.

Spot name	Fm	Domain	SiO2	P2O5	Y2O3	CaO	La2O3	Pr2O3	Nd2O3	Sm2O3	Ce2O3	ThO2	PbO	UO2	Total	Age (Ma)	2σ err
KA-95-Mnz-01	BI-d2	rim	1.1431	28.0864	0.4481	1.5529	9.4227	3.2463	2.9807	6.2649	30.1857	3.1045	0.1583	0.0944	86.6880	1051	138
KA-97-Mnz-02	BI-d1	incl in xen	1.4592	28.5431	1.8318	0.2061	12.0875	2.1577	3.0555	5.5195	29.7221	3.4445	0.2201	0.2628	88.5099	1149	123
KA-97-Xen-01	BI-d1	rim	0.5663	28.4950	34.2522	0.0329	0.0093	0.0000	NM	0.5507	0.0554	0.7791	0.0871	0.3288	65.1568	1039	219
KA-97-Xen-02	BI-d1	rim-core	0.5120	28.3649	34.1646	0.0131	0.0000	0.0000	NM	0.5178	0.0542	0.7263	0.1514	0.6835	65.1878	1115	167
KA-97-Xen-02	BI-d1	core	0.4217	29.7827	37.5154	0.0140	0.0042	0.0190	NM	0.4801	0.0490	0.4683	0.1095	0.4845	69.3484	1158	229
KA-97-Xen-02	BI-d1	core	0.9183	30.4984	38.0817	0.0323	0.1011	0.0000	NM	0.7842	0.3543	0.9023	0.2054	0.8868	72.7648	1172	122
LU-149(1)-Mnz-01	BI-e1	–	1.1572	26.3722	0.1892	1.0546	21.2277	0.6578	3.5475	0.9097	29.3927	3.2056	0.2627	0.0619	88.0388	1697	160
LU-149(1)-Mnz-01	BI-e1	–	1.2860	26.7546	0.1737	1.1274	21.8908	0.6865	3.7366	0.9176	29.9070	3.1571	0.2615	0.0646	89.9634	1708	162
LU-149(1)-Mnz-01	BI-e1	–	1.4051	27.0560	0.1710	1.0650	22.2925	0.6337	3.8916	0.9222	29.9099	3.1202	0.2676	0.0593	90.7941	1775	167
LU-60-Mnz-01-1	BI-c2	–	0.4179	26.7196	2.1146	0.8916	13.0944	2.2054	4.0098	2.2380	27.0700	3.5008	0.2999	0.4466	83.0086	1312	105
LU-60-Mnz-01-2	BI-c2	–	0.6994	29.8469	1.2712	0.8149	13.3493	2.1384	4.0279	2.2440	27.6862	3.6995	0.3589	0.7350	86.8716	1268	86
LU-60-Mnz-01-3	BI-c2	–	1.1327	18.1755	2.0859	1.4161	12.7848	1.9460	4.1271	1.9913	23.8139	3.6109	0.3877	0.8547	72.3266	1300	80
LU-60-Mnz-03-1	BI-c2	–	0.3285	27.4330	2.0674	1.4929	13.0636	1.9641	4.3294	2.1700	25.9641	4.6941	0.4575	0.9001	84.8647	1292	71
LU-60-Mnz-03-2	BI-c2	–	0.8682	27.2456	2.4759	1.5961	12.0589	1.8147	3.9465	2.3022	25.9993	4.3889	0.4734	1.0878	84.2575	1279	68
LU-60-Mnz-04-1	BI-c2	–	0.7302	26.4355	0.5986	0.8488	12.7899	2.1230	2.7777	1.4352	25.9333	4.0004	0.2329	0.1346	78.0401	1156	118
LU-60-Mnz-04-2	BI-c2	–	1.2067	27.7283	1.2627	0.7738	12.5935	2.1078	2.8929	1.2417	25.2262	3.4507	0.2149	0.1051	78.8043	1249	138

Errors and detection limits on Th, U and Pb are calculated using the statistical approach of Ancey et al. (1978). Errors are given at ± 2σ (with 95% confidence level; Montel et al., 1996; Jercinovic and Williams, 2005).

Analyzes were performed with a Cameca SX-Five Electron Microprobe equipped with five wavelength-dispersive spectrometers (WDS) at Camparis (UPMC, Paris). The operating conditions were 15 kV accelerating voltage and 100 nA beam current. The analyzed elements are: Si and P (Kα line with a TAP monochromators), Ca (Kα line with a PET monochromators), Y, La, Ce and Sm (Lα line with a PET monochromators). Monazites and xenotimes can also contain Tb, Dy, Ho, Er, Tm, Yb, Lu, and F, which explain why the total (in% wt) is not equal to 100 in Table 2. However, these elements are not used to calculate the U-Th-Pb age. Four of the five available WDS were set with PET monochromators (two with a regular area, 22×32 mm², and two with a large area, 22×60 mm²). They were operated simultaneously to analyze successively, U (Mβ line), Th (Mα line) and Pb (Mβ line). Standards are ThO2 for Th, UO2 for U, PbS for Pb, Durango apatite for P and Ca, two rare earth doped glasses for Y, La, Ce and Sm and diopside for Si. The counting time was set at 20 s (peak + background) for all elements except U, Th and Pb for which 600 s was taken to reduce uncertainties. Measured ages are corrected using the reference monazite from Thompson Mine, Manitoba, Canada (TM, 1766 Ma). Maps are obtained using a focused beam in rastering mode, with a step size of 0.3 μm and a dwell time of 250 ms per pixel.

5.2. U-Pb dating with LA-ICP-MS

U-Th-Pb geochronology of monazite, xenotime and zircon was conducted by Laser Ablation Inductively Coupled with Plasma Mass Spectrometry at the Laboratoire Magmas et Volcans, Clermont-Ferrand (France). The analyzes involve the ablation of minerals with a Resonetics Resolution M-50E powered by an ultra-short pulse ATL Atlex Excimer laser system operating at a wavelength of 193 nm. Spot diameters of 12 μm (zircons) and 7 μm (monazites and xenotimes) associated to repetition rates of 3 and 2 Hz with laser energy of 3 and 2.5 mJ were used respectively for zircon and monazite/xenotime. The ablated material is carried into helium, and then mixed with nitrogen and argon, before injection into a plasma source of an Agilent 7500 cs ICP-MS equipped with a dual pumping system to enhance the sensitivity (Paquette et al., 2014). The analytical method is basically similar to that developed by and reported in Paquette and Tiepolo (2007) and Hurai et al. (2010). The signals of ^{204}(Pb + Hg), ^{206}Pb, ^{207}Pb, ^{208}Pb, ^{232}Th and ^{238}U masses are acquired. The occurrence of common Pb in the sample can be monitored by the evolution of the ^{204}(Pb + Hg) signal intensity, but no common Pb correction was applied owing to the large isobaric interference from Hg. The ^{235}U signal is calculated from ^{238}U on the basis of the ^{238}U/^{235}U = 137.88. Single analyzes consisted of 30 s of background integration with laser off followed by 1 min integration with the laser firing. Data are corrected for U–Pb and Th–Pb fractionation occurring during laser sampling and for instrumental mass discrimination (mass bias) by standard bracketing with repeated measurements of GJ-1 zircon (Jackson et al., 2004) and Trebilcock monazite standards (Tomascak et al., 1996). Data reduction was carried out with the software package GLITTER® (developed by the Macquarie Research Ltd.; Van Achterbergh et al., 2001). For each analysis, the time-resolved signal of single isotopes and isotopic ratios was monitored and carefully inspected to verify the presence of perturbations related to inclusions, fractures, mixing

Table 3

LA-ICP-MS monazite and xenotime U-Th-Pb isotope data for BI Group.

Spot Name	Formation	Domain	Pb (ppm)	Th (ppm)	U (ppm)	Th/U	207Pb/235U	2σ err	206Pb/238U	2σ err	ρ	208Pb/232Th age (Ma)	2σ err	207Pb/206Pb age (Ma)	2σ err	206Pb/238U age (Ma)	2σ err	Concord. %
KA-80-Xen-02	BI-E2	–	289	707	663	1.1	2.265	0.079	0.164	0.004	0.71	1229	31	1633	74	976	23	60
KA-80-Xen-02	BI-E2	–	376	874	859	1.0	2.923	0.102	0.169	0.004	0.72	1098	29	2037	71	1005	24	49
KA-80-Xen-02	BI-E2	–	118	83	159	0.5	5.381	0.239	0.306	0.009	0.63	2582	93	2066	86	1720	42	83
KA-80-Xen-02	BI-E2	–	402	604	822	0.7	3.487	0.110	0.189	0.005	0.79	1694	42	2151	64	1115	26	52
KA-80-Mnz-05	BI-E2	core	4138	35402	2685	13	2.071	0.060	0.175	0.004	0.84	979	22	1338	66	1038	23	78
KA-80-Mnz-03	BI-E2	core	340	2550	101	25	2.242	0.126	0.192	0.006	0.51	1312	30	1313	116	1130	30	86
KA-80-Mnz-07	BI-E2	core	404	4478	64	70	3.310	0.216	0.198	0.007	0.51	973	23	1978	122	1163	35	59
KA-80-Mnz-11	BI-E2	core	141	727	33	22	6.949	0.413	0.341	0.012	0.57	1797	44	2320	108	1892	55	82
KA-80-Mnz-14	BI-E2	–	11234	73396	11899	6.2	2.055	0.062	0.179	0.005	0.85	1061	25	1280	66	1059	25	83
KA-80-Mnz-14	BI-E2	–	9626	62380	9179	6.8	2.137	0.065	0.186	0.005	0.84	1127	27	1277	67	1100	26	86
KA-80-Mnz-14	BI-E2	–	8096	47463	8527	5.6	2.165	0.067	0.189	0.005	0.84	1160	28	1270	66	1116	26	88
KA-80-Mnz-14	BI-E2	–	8530	51024	7854	6.5	2.174	0.068	0.192	0.005	0.83	1158	28	1253	67	1129	27	90
KA-83-Xen-01	BI-E2	core	147	108	274	0.4	2.894	0.121	0.229	0.006	0.66	1397	54	1461	86	1329	33	91
KA-83-Xen-01	BI-E2	rim	519	533	1060	0.5	2.423	0.070	0.211	0.005	0.87	1050	28	1280	65	1231	29	96
KA-83-Xen-02	BI-E2	core	3251	809	4407	0.2	5.466	0.143	0.332	0.008	0.96	1639	41	1946	55	1850	40	95
KA-83-Xen-03	BI-E2	rim	3782	1138	7019	0.2	3.146	0.082	0.248	0.006	0.96	1541	38	1471	59	1426	32	97
KA-83-Xen-03	BI-E2	rim	3883	1221	7592	0.2	3.013	0.079	0.235	0.006	0.96	1492	37	1491	58	1358	31	91
KA-83-Mnz-02	BI-E2	core	4229	41660	935	45	1.941	0.056	0.180	0.005	0.88	1113	19	1148	66	1069	16	93
KA-83-Mnz-02	BI-E2	core	3591	37170	837	44	2.024	0.062	0.186	0.005	0.83	1051	27	1174	69	1098	25	94
KA-83-Mnz-07	BI-E2	core	1418	18892	268	70	1.783	0.108	0.142	0.004	0.51	827	25	1443	121	858	26	59
KA-83-Mnz-09	BI-E2	core	8728	91748	1889	49	1.870	0.054	0.169	0.004	0.87	1018	20	1205	66	1006	25	83
KA-83-Mnz-11	BI-E2	core	897	9108	202	45	2.891	0.109	0.215	0.006	0.70	1018	24	1580	78	1254	30	79
KA-83-Mnz-12	BI-E2	core	1742	20454	238	86	1.618	0.069	0.128	0.004	0.64	945	23	1460	88	777	20	53
KA-84-Mnz-02	BI-E2	core	1342	15092	351	43	2.254	0.085	0.195	0.005	0.69	917	21	1289	82	1148	27	89
KA-84-Mnz-03	BI-E2	core	1138	7480	342	22	6.623	0.193	0.372	0.009	0.86	1335	30	2087	60	2038	43	98
KA-84-Mnz-04	BI-E2	core	2286	23760	674	35	2.015	0.064	0.174	0.004	0.78	1003	23	1292	71	1035	24	80
KA-84-Mnz-05	BI-E2	rim	3427	17965	4134	4.4	2.473	0.067	0.201	0.005	0.90	1094	25	1409	62	1181	26	84
KA-84-Mnz-05	BI-E2	core	2745	16408	2920	5.6	2.673	0.071	0.204	0.005	0.91	1053	24	1527	61	1198	26	78
KA-84-Mnz-06	BI-E2	core	5086	28977	716	40	5.743	0.159	0.347	0.008	0.87	1776	39	1955	60	1922	40	98
KA-84-Mnz-07	BI-E2	core	2363	21076	238	89	5.228	0.190	0.296	0.008	0.72	1201	27	2074	73	1670	38	81
KA-84-Mnz-08	BI-E2	core	2652	15410	1136	14	4.796	0.133	0.291	0.007	0.87	1426	31	1952	60	1644	35	84
KA-84-Mnz-09	BI-E2	rim	3672	28094	1041	27	2.744	0.076	0.230	0.006	0.86	1282	28	1353	65	1333	29	98
KA-84-Mnz-09	BI-E2	rim	3294	27446	693	40	2.761	0.079	0.228	0.006	0.84	1226	27	1375	66	1326	29	96
KA-84-Mnz-11	BI-E2	core	2165	14667	143	102	6.796	0.249	0.368	0.010	0.71	1612	35	2150	73	2021	45	94
KA-84-Mnz-13	BI-E2	rim	6521	28638	610	47	12.577	0.347	0.479	0.011	0.86	2313	49	2746	55	2523	50	92
KA-84-Mnz-13	BI-E2	rim	10661	43634	878	50	13.705	0.395	0.510	0.012	0.84	2482	53	2783	57	2658	53	96
KA-84-Mnz-16	BI-E2	core	5636	39189	349	112	5.370	0.171	0.317	0.008	0.77	1579	34	1998	66	1775	38	89
KA-95-Xen-01	BI-d2	core	885	5316	1411	3.8	1.945	0.058	0.177	0.004	0.83	741	17	1189	68	1051	24	88
KA-95-Xen-02	BI-d2	core	289	891	676	1.3	1.561	0.063	0.154	0.004	0.64	794	22	1029	89	923	22	90
KA-97-Xen-02	BI-d1	core	1172	8129	390	21	2.758	0.088	0.227	0.006	0.78	1398	32	1384	71	1320	30	95
KA-97-Xen-02	BI-d1	core	1016	3151	1897	1.7	1.967	0.058	0.177	0.004	0.83	1029	24	1217	68	1048	24	86
KA-97-Xen-01	BI-d1	core	629	3086	1126	2.7	2.190	0.071	0.179	0.004	0.77	697	17	1403	72	1060	24	76
KA-97-Xen-03	BI-d1	–	3107	3642	5989	0.6	2.346	0.060	0.204	0.005	0.94	1276	29	1275	61	1199	26	94
KA-97-Xen-03	BI-d1	–	3779	3646	7852	0.5	2.201	0.056	0.192	0.005	0.93	1279	29	1274	61	1132	25	89
KA-97-Xen-03	BI-d1	–	3280	2776	7408	0.4	2.075	0.054	0.182	0.004	0.92	1086	26	1260	62	1079	24	86
KA-97-Xen-03	BI-d1	–	3324	3428	7208	0.5	2.121	0.055	0.185	0.004	0.93	1153	27	1274	61	1094	24	86
KA-97-Xen-Zr-17	BI-d1	rim	2178	5430	3876	1.4	2.451	0.063	0.202	0.005	0.93	904	21	1382	60	1187	26	86
KA-97-Xen-Zr-17	BI-d1	rim	740	2495	1220	2.1	2.486	0.072	0.208	0.005	0.84	807	19	1355	66	1218	27	90
LU-69-Mnz-04	BI-c2	rim	5202	27908	4804	5.8	2.529	0.068	0.215	0.005	0.93	1245	29	1320	62	1257	28	95
LU-69-Mnz-04	BI-c2	rim	5400	30953	4932	6.3	2.433	0.066	0.206	0.005	0.92	1209	28	1327	62	1210	27	91
LU-69-Mnz-05	BI-c2	rim	2589	18793	1086	17	2.607	0.076	0.223	0.006	0.86	1264	30	1315	66	1295	29	99
LU-69-Mnz-05	BI-c2	core	2884	22645	954	24	2.662	0.081	0.222	0.006	0.83	1229	29	1363	67	1291	30	95
LU-69-Mnz-08	BI-c2	rim	913	5620	444	13	2.815	0.092	0.223	0.006	0.78	1420	33	1460	70	1297	30	89

Table 3 (continued)

Spot Name	Formation	Domain	Pb (ppm)	Th (ppm)	U (ppm)	Th/U	$^{207}Pb/^{235}U$	2σ err	$^{206}Pb/^{238}U$	2σ err	ρ	$^{208}Pb/^{232}Th$ age (Ma)	2σ err	$^{207}Pb/^{206}Pb$ age (Ma)	2σ err	$^{206}Pb/^{238}U$ age (Ma)	2σ err	Concord. %
LU-69-Mnz-08	BI-2	rim	2238	15722	1286	12	2.667	0.081	0.214	0.005	0.83	1200	28	1432	67	1251	29	87
LU-69-Mnz-02	BI-2	core	465	4294	267	16	2.205	0.092	0.179	0.005	0.64	1013	24	1416	87	1059	26	75
LU-69-Mnz-07	BI-2	core	4932	50131	1611	31	2.532	0.075	0.200	0.005	0.85	1012	24	1464	65	1175	27	80
LU-69-Mnz-13	BI-2	core	9858	44781	751	60	11.787	0.324	0.443	0.011	0.91	2338	53	2769	53	2362	49	85
LU-69-Mnz-13	BI-2	rim	9557	46422	303	153	11.128	0.315	0.430	0.011	0.89	2295	52	2723	55	2305	49	85
LU-69-Mnz-19	BI-2	core	1241	5272	1170	4.5	2.887	0.086	0.234	0.006	0.84	1482	34	1417	65	1354	31	96
LU-69-Mnz-03	BI-2	rim	7927	54588	5888	9.3	2.632	0.072	0.202	0.005	0.90	1169	27	1520	61	1185	27	78
LU-60-Mnz-03	BI-2	rim	7932	54291	5826	9.3	2.522	0.069	0.204	0.005	0.90	1171	27	1418	62	1197	27	84

of different age domains or common Pb. Calculated ratios were exported, and Concordia ages and diagrams were generated using the Isoplot/Ex v. 2.49 software package by Ludwig (2001). The analytical data are provided in Tables 34 where errors are given at ± 2σ. In the text and figures, all uncertainties in ages are given at the 2σ level. The discordant data were considered only if they allowed possible Discordia lines to be defined on the Concordia diagrams; otherwise they were not taken into account because of doubtful interpretation. In laser-ablation ICPMS analyzes several factors that cannot be easily detected from the inspection of the time-resolved signals might contribute to discordance (e.g. common Pb, mixing of different age domains, small cracks or inclusions). The concentrations in U-Th-Pb were calibrated relative to the certified contents of GJ-1 zircon (Jackson et al., 2004) and Trebilcock monazite standards (Tomascak et al., 1996).

6. Results

6.1. Electron MicroProbe

A total of 6 monazites and 1 xenotime with a monazite inclusion (Table 2; Fig. 4) were used for *in situ* EMP analyzes. Ages (corrected using a reference monazite) vary from 1039 to 1775 Ma. The youngest ages obtained on a small monazite (Fig. 4a; 15×5 µm), and on a xenotime (Fig. 4b) from the Kafuku drill core were 1051 ± 138 Ma and 1039 ± 219 Ma respectively. This xenotime mineral shows different zonations and the younger age was only obtained in the external rim. The internal rim and a monazite inclusion are dated around 1150–1170 Ma, even if the errors are very large (2σ: 120 to 220 Myr). However these results are confirmed by the age obtained by LA-ICP-MS on the internal rim of xenotime at 1217 ± 68 Ma (error is 2σ). To better constrain the ages of the external rims, we performed X-rays maps (Th Mα, Pb Mβ and U Mβ) on 6 monazites from Lubi and Kafuku drill cores (Figs. 5 and 6). We calculated a mean age and its associated error (1σ; Fig. 5) for 10 points of external rims of each monazite. Results clearly highlight that monazites display zonations with external rims between 1049 ± 29 Ma and 1061 ± 20 Ma. In Fig. 6, two whole age populations (core *vs* rim) are graphically presented with a standard normal distribution presentation, corresponding to the pixel values from blue and green boxes respectively. Mean ages and their associated errors are calculated on the two age populations. Thus, the core mean age is around 1143–1152 Ma (n = 120) and the rim mean age is around 1040–1065 Ma (n = 200). This confirm results deduced from the Figs. 4 and 5 and results from François et al. (2016).

6.2. LA-ICP-MS

6.2.1. Monazites and xenotimes

A total of 30 monazites and 9 xenotime are used for *in situ* U-Pb dating with LA-ICP-MS analyzes (Table 3; Figs. 7a, b and 8a). Results provide $^{207}Pb/^{206}Pb$ ages between 2783 and 1148 Ma for monazites and between 2151 and 1029 Ma for xenotimes. Three age groups stand out, the first between 1000 and 1700 Ma (74% of monazites and xenotimes), the second between 1900 and 2400 Ma (20%) and the third between 2700 and 2800 Ma (6%). Only monazite grains have an age between 2300 and 2800 Ma. Overall, xenotimes are younger than monazites, and the youngest age occurs in a Kafuku xenotime crystal (Figs. 7a and 8a). The Kafuku drill cores display a widest range of values; ages between 1900 and 2400 Ma are only recorded in this core as well as values below 1300 Ma (Fig. 8a).

Table 4
LA-ICP-MS zircon U–Th–Pb isotope data for BI & BII Group.

| Spot Name	Formation	Domain	Pb (ppm)	Th (ppm)	U (ppm)	Th/U	$^{207}Pb/^{235}U$	2σ err	$^{206}Pb/^{238}U$	2σ err	ρ	$^{207}Pb/^{206}Pb$ age (Ma)	2σ err	$^{206}Pb/^{238}U$ age (Ma)	2σ err	Conc
LU-149 (1)-Zr-12	BI-e1	core	210	806	1001	0.8	3.532	0.092	0.199	0.005	0.89	2077	57	1172	25	56
LU-149 (1)-Zr-14	BI-e1	rim	194	186	416	0.5	11.916	0.298	0.429	0.010	0.92	2838	52	2301	44	81
LU-149 (1)-Zr-14	BI-e1	rim	67	142	165	0.9	9.880	0.26	0.362	0.008	0.89	2808	54	1993	40	71
LU-149 (1)-Zr-22	BI-e1	rim	11	30	36	0.8	4.402	0.19	0.252	0.007	0.62	2054	85	1447	35	70
LU-149 (1)-Zr-22	BI-e1	core	16	47	61	0.8	4.031	0.138	0.221	0.005	0.72	2130	70	1286	29	60
LU-149 (1)-Zr-24	BI-e1	rim	66	149	503	0.3	1.916	0.05	0.121	0.003	0.88	1876	59	737	16	39
LU-149 (1)-Zr-24	BI-e1	rim	112	171	767	0.2	2.092	0.053	0.139	0.003	0.89	1786	59	838	18	47
LU-149 (1)-Zr-28	BI-e1	rim	140	490	1119	0.4	2.062	0.053	0.112	0.003	0.89	2138	57	687	15	32
LU-149 (1)-Zr-38	BI-e1	core	412	449	1760	0.3	5.017	0.127	0.220	0.005	0.89	2508	55	1284	26	51
LU-149 (1)-Zr-38	BI-e1	rim	258	280	1341	0.2	3.852	0.098	0.181	0.004	0.88	2397	55	1071	22	45
LU-149 (1)-Zr-36	BI-e1	rim	23	39	85	0.5	3.312	0.098	0.245	0.006	0.77	1591	68	1410	29	89
LU-149 (1)-Zr-36	BI-e1	rim	39	83	161	0.5	3.115	0.085	0.229	0.005	0.83	1598	64	1330	27	83
LU-149 (1)-Zr-40	BI-e1	core	270	304	847	0.4	6.115	0.153	0.306	0.007	0.88	2290	56	1719	33	75
LU-149 (2)-Zr-02	BI-e1	rim	156	260	296	0.9	12.123	0.314	0.419	0.009	0.87	2906	54	2254	43	78
LU-149 (2)-Zr-02	BI-e1	rim	159	200	293	0.7	12.940	0.337	0.446	0.010	0.86	2910	54	2376	45	82
LU-149 (2)-Zr-02	BI-e1	core	98	227	202	1.1	11.068	0.293	0.381	0.009	0.85	2911	55	2081	40	71
LU-149 (2)-Zr-09	BI-e1	core	21	57	91	0.6	2.949	0.092	0.215	0.005	0.73	1612	70	1257	26	78
LU-149 (2)-Zr-12	BI-e1	core	26	80	80	1.0	4.578	0.141	0.273	0.006	0.74	1978	68	1557	31	79
LU-149 (2)-Zr-12	BI-e1	rim	26	101	87	1.2	3.988	0.13	0.240	0.006	0.71	1967	70	1384	29	70
LU-149 (2)-Zr-06	BI-e1	core	108	124	485	0.3	3.185	0.084	0.217	0.005	0.82	1737	63	1267	25	73
LU-149 (2)-Zr-04	BI-e1	core	100	449	319	1.4	4.356	0.119	0.238	0.005	0.79	2138	61	1373	27	64
LU-149 (2)-Zr-04	BI-e1	rim	90	315	407	0.8	3.599	0.099	0.193	0.004	0.78	2164	62	1139	23	53
KA-83-Zr-01	BI-E2	core	66	626	701	0.9	1.178	0.045	0.079	0.002	0.68	1769	77	490	12	28
KA-83-Zr-02	BI-E2	core	49	208	247	0.8	1.927	0.066	0.160	0.004	0.73	1371	74	955	22	70
KA-83-Zr-03	BI-E2	core	34	101	133	0.8	3.912	0.141	0.222	0.006	0.72	2070	72	1291	30	62
KA-83-Zr-04	BI-E2	rim	93	674	992	0.7	1.271	0.039	0.084	0.002	0.80	1794	66	520	12	29
KA-83-Zr-04	BI-E2	rim	113	385	807	0.5	1.942	0.06	0.129	0.003	0.80	1793	65	779	18	43
KA-83-Zr-06	BI-E2	core	39	93	220	0.4	3.040	0.108	0.167	0.004	0.71	2123	71	997	23	47
LU-60-Zr-05	BI-c2	rim	52	567	253	2.2	2.017	0.058	0.148	0.003	0.81	1605	65	889	19	55
LU-60-Zr-14-2	BI-c2	core	13	28	38	0.7	5.153	0.173	0.281	0.007	0.72	2140	69	1595	34	75
LU-60-Zr-14-2	BI-c2	rim	23	49	71	0.7	4.193	0.128	0.282	0.007	0.76	1764	67	1600	33	91
LU-60-Zr-14-1	BI-c2	rim	50	330	376	0.9	1.678	0.047	0.126	0.003	0.79	1561	66	764	16	49
LU-69-Zr-11	BI-c2	core	19	190	185	1.0	1.094	0.042	0.089	0.002	0.62	1406	84	550	13	39
LU-69-Zr-09	BI-c2	core	125	553	780	0.7	2.064	0.055	0.142	0.003	0.83	1729	62	853	18	49
LU-69-Zr-21	BI-c2	rim	33	149	173	0.9	2.202	0.074	0.176	0.004	0.69	1437	76	1047	22	73
LU-69-Zr-07	BI-c2	core	40	98	206	0.5	2.318	0.064	0.184	0.004	0.80	1456	66	1088	22	75
LU-69-Zr-15	BI-c2	rim	33	49	160	0.3	2.401	0.073	0.208	0.005	0.74	1284	73	1219	25	95
LU-69-Zr-15	BI-c2	core	32	54	141	0.4	2.581	0.075	0.222	0.005	0.77	1303	70	1290	26	99
LU-69-Zr-01	BI-c2	core	17	202	182	1.1	1.160	0.054	0.084	0.002	0.54	1636	96	518	13	32
LU-69-Zr-03	BI-c2	core	13	102	61	1.7	2.405	0.14	0.152	0.004	0.50	1881	114	910	24	48
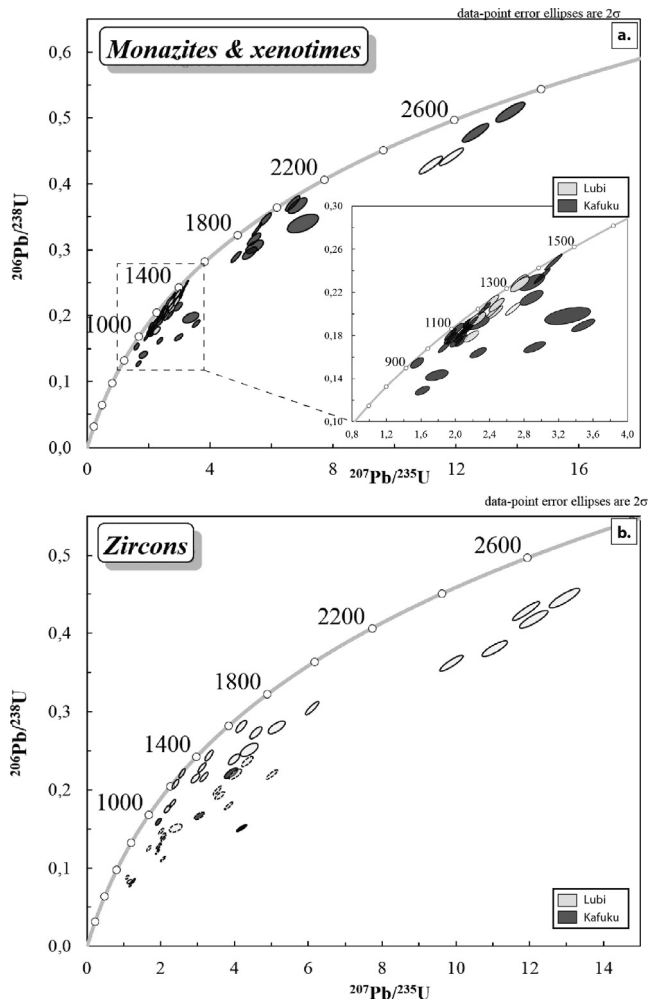
Fig. 8. Concordia diagrams for LA-ICP-MS U-Th-Pb analyzes on (a) 30 monazite and 9 xenotime grains (43 and 18 analyzes respectively) with inset between 900 and 1500 Ma and (b) 28 zircons (40 analyzes, dotted ellipses represent analyzes with a concordance lower than 70%). Error ellipses are 2σ.

6.2.2. Zircons

A total of 28 zircons are used (Table 4; Fig. 8b). They show a weak oscillatory zoning (Fig. 7c) and a systematically high Th/U ratio (0.13–2.24) regardless of the variable amounts of U (36–1760 ppm) and Th (28–806 ppm) testifying inherited magmatic or metamorphic (for the low Th/U ratio) origins. Zircon ages obtained are highly discordant with a fan distribution and are poorly constrained, possibly because the system was reopened during the metamorphic and magmatic events. This highlights metamict zircons that lost radiogenic Pb and gained common Pb. Nevertheless, they provide $^{207}Pb/^{206}Pb$ ages between 2911 and 1284 Ma (Fig. 6). The youngest zircon yields a $^{207}Pb/^{206}Pb$ apparent age at 1284 Ma and is located in Lubi drill core (Fig. 6).

7. Discussion

7.1. Set of inherited ages

Our $^{206}Pb/^{238}U$ zircon ages are highly discordant and no age trend is identified. Moreover, $^{207}Pb/^{206}Pb$ ages are not significant due to the presence of common Pb. Given these results, we propose to perform a compilation of previous U-Pb geochronological

studies in the region, and compare it with our ages. Fig. 9 summarizes previous U-Pb geochronological studies in the region from Batumike et al., 2009; Fig. 9a), Delpomdor et al. (2013; Fig. 9b) and from this study (Fig. 9c) together with a compilation of all these studies (Fig. 9d). In Batumike et al. (2009), 127 zircon grains were analyzed from the Luebo region (Fig. 9a) close to rivers which cut through the Mbuji-Mayi Supergroup. Most of analyzes are concordant. The oldest zircon gives an age of 3235 ± 7 Ma. Late-Archean zircons have ages ranging between 2903 and 2530 with two main populations grouped at 2890 ± 8 Ma and 2620 ± 10 Ma. Paleoproterozoic zircons show three populations at 2390 ± 20, 2150 ± 5 and 2070 ± 9 Ma. Rare zircons have ages between 2000 and 1150 Ma, there is maybe a small population in the Mesoproterozoic at 1441 ± 17 Ma (n = 4) and 1060 ± 14 Ma (n = 6). There is a spread of ages from the Mesoproterozoic–Neoproterozoic transition to the end of the Neoproterozoic, with an important population observed around 608 ± 5 Ma. Another age group is observed at 493 Ma (n = 14). In the second study (Delpomdor et al., 2013), 355 zircon grains were analyzed from siliciclastic rocks belonging to the BI Group in two samples from Kafuku drill core (RG41375, BId2 and RG41382, BId2), and in two samples from Lubi drill core (RG57673, BId2 and RG57809, BIc1). 165 of 336 analyzes are concordant and used for the probability plot (Fig. 9b). Three main peaks are highlighted between *ca.* 1.1 and 1.4 Ga, 1.7 and 2.1 Ga, and 2.7 and 2.9 Ga.

Our dating is concordant with these previous studies (Fig. 9c and d) albeit less of data and except without ages older than 3.0 Ga and younger than 1.0 Ga, and allow to define the different origin of the sediments constituting the lower part of the Mbuji-Mayi Supergroup:

(i) Ages between 2.6 and 2.8 Ga correspond to the age of intrusion of Dibaya granitic and migmatitic Complex (Northern part of Congo-Kasai Craton) and are compatible with results of Delhal et al. (1975), Cahen et al. (1984) and Delpomdor et al. (2013).

(ii) Ages between 1.9 and 2.4 Ga are scattered but consistent with the Luiza metasedimentary Complex (Delhal and Ledent, 1973; Delhal and Ladmirant, 1979; Cahen et al. 1984), where a thermo-tectonic event is recorded between 2.0 and 2.2 Ga (Rb-Sr on micas from granites and pegmatites; Delhal and Ledent, 1973). It could be also consistent with the Lulua Complex, probably older than 1468 ± 30 Ma (Snelling, unpublished data) and around 2.0–2.2 Ga (K-Ar; Delhal and Ladmirant, 1979).

(iii) The age peak around 1.8–1.9 Ga corresponds to a system of Palaeoproterozoic belts, respectively on the southeastern margin of the Tanzania Craton (Usagara Belt), and between the Bangweulu Block and Tanzania Craton (Ubende Belt; de Waele et al., 2008). It results from an important tectonothermal event during the amalgamation of the Tanzania Craton and the Bangweulu Block (Lenoir et al., 1994; Möller et al., 1995; Boven et al., 1999; Reddy et al., 2003; Collins et al., 2004; Sommer et al., 2005).

(iv) Ages between 1.1 and 1.7 Ga are coeval with the Kibara orogenic cycle occurring during convergence between the Tanzania-Bangweulu Craton and the Congo-Kasai Craton (Cahen et al., 1984; De Waele, 2004; Johnson et al., 2005; De Waele and Fitzsimons, 2007; Begg et al., 2009; Fernandez-Alonso et al., 2012), with a plutonic activity peak at 1.3–1.4 Ga (Tack et al., 2002; Kokonyangi et al., 2004, 2006, 2007; Tack et al., 2010).

Archean ages between 2.6 and 2.8 Ga are clearly recorded in the Lubi samples (Figs. 9b–d and 10c in green) and in the Luebo region (Figs. 9a, d and 10b in yellow) due to the proximity with the Dibaya
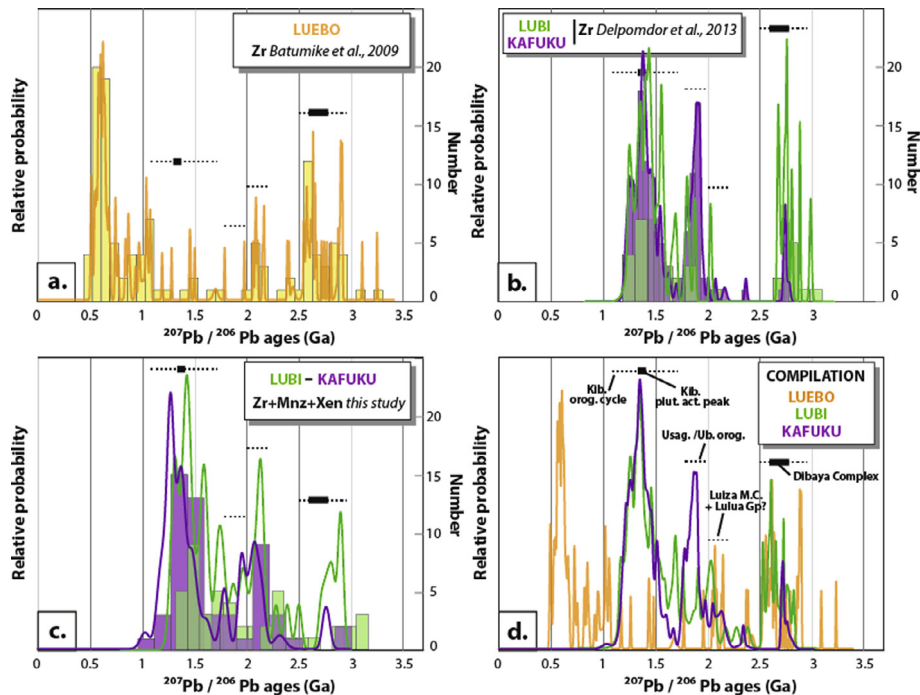
Fig. 9. ^{207}Pb/^{206}Pb apparent ages (Ga) on (a) zircons from the Luebo region (Batumike et al., 2009), (b) zircons from the Kafuku and Lubi drill cores (Delpomdor et al., 2013) and (c) xenotimes, monazites and zircons from the Kafuku and Lubi drill cores (*this study*). (d) Compilation of all ^{207}Pb/^{206}Pb apparent ages (Ga). Kibara plutonic activity peak, Kibara orogenic cycle, Usagara/Ubende orogeny, Luiza Metasedimentary Complex and Lulua Group.

Complex (Fig. 10a). The Ubende/Usagara (1.8–1.9 Ga) and Kibara (1.1–1.7 Ga) ages are preferentially found in the Kafuku samples (Figs. 9b, c and 10d in purple) located in the southeastern part of the Mbuji-Mayi area (Fig. 10a). The quasi-absence of zircons with ages of 1.8–1.9 Ga and 1.3–1.4 Ga in the Luebo region (Fig. 10b) clearly indicates that these zircons did not come from the eastern margin, where rocks of these ages (Paleoproterozoic Bangweulu Block and Mesoproterozoic Kibara Belt) are known (Batumike et al., 2009).

Furthermore, the source of sediments has changed over time within the Lubi and the Kafuku drill cores (Fig. 11). In the Lubi drill core, we observe a probable unique Archean Congo-Kasai source in the BIc1 Formation followed by a dominantly Kibara source in the BIc2 Formation, and again Archean and Kibara sources with minor Usagara and Ubende contributions in the BId2 Formation. The sediments increasingly come from a remote easterly source, more than 400 km away. Also, an important supply of sediments in the BIe1 Formation came from the Lulua and Luiza complexes while the proportion of sediments from the Kibara Belt was strongly decreasing. In the Kafuku drill core, the BId1 Formation was marked by a probable Kibara supply, while the BId2 Formation deposit (Lower and Upper) recorded also an important Usagara and Ubende source with minor Congo-Kasai source. The BIE2 Formation showed, with an Archean, a Usagara/Ubende and a Kibara sources, also a contribution from the Lulua and Luiza complexes. This was probably due to the hiatus of the BIE in the Lubi drill core and a more distant sediment supply from the WSW (Fig. 10a). Thus, sediments from the Mbuji-Mayi area indicate a multiple provenance from the Dibaya Complex/Congo-Kasai Craton and from the network of belts to the east/southeast (Fig. 10). These dating highlight a complex provenance for sediments composing the BI Group with poly-magmatic and -metamorphic origins. This also testifies, between Lubi and Kafuku, the presence of natural barriers at the boundary between the continent and the sedimentary basin

which temporarily blocked the supply of sediments from a given source.

7.2. Diagenesis of Mbuji-Mayi Supergroup

U-Pb ages obtained on sediment from the Mbuji-Mayi Supergroup by Delpomdor et al. (2013) suggest a maximum age at 1175 Ma for the beginning of BI Group diagenesis. Our results with EMP on the Kafuku and Lubi drill cores clearly highlight younger ages (between 1039 and 1065 Ma; Figs. 4–6 and 11) obtain on external rims of monazites and xenotimes, probably corresponding to a recrystallization during diagenesis. These results are confirmed with ^{207}Pb/^{206}Pb age at 1029 Ma obtain on a xenotime with LA-ICP-MS (Figs. 7a and 8a). Thus, we propose a diagenesis of BI Group younger than 1175 Ma and probably around 1030–1065 Ma. This confirms previous Pb-Pb ages obtained on syngenetic galena around 1055 Ma (BI Group; Cahen, 1954; Holmes and Cahen, 1955; Raucq, 1957) and correlation of Bertrand-Sarfati (1972) with series of Mauritania dating the BII Group deposit, overlying the BI Group, between 1019 ± 36 Ma and 909 ± 37 Ma (isochron ages by Bonhomme and Clauer, 1972; Clauer, 1973). Dating on basaltic pillow lavas topping the Mbuji-Mayi Supergroup (Cahen et al., 1974 and Cahen et al., 1984) limit in time the end of sedimentary deposit of this Supergroup before 950 Ma. Moreover, the exceptionally diverse and well-preserved organic-walled microfossil assemblage from the Mbuji-Mayi Supergroup and comparison with other worldwide microfossil assemblages shows that the Mbuji-Mayi assemblage is likely Late Mesoproterozoic–Early Neoproterozoic (Baludikay et al., 2016a), consistent also with our geochronological data.

7.3. Implications for eukaryotic diversification in Central Africa

Proterozoic microfossils constitute a major source of paleontological information essential for understanding early life
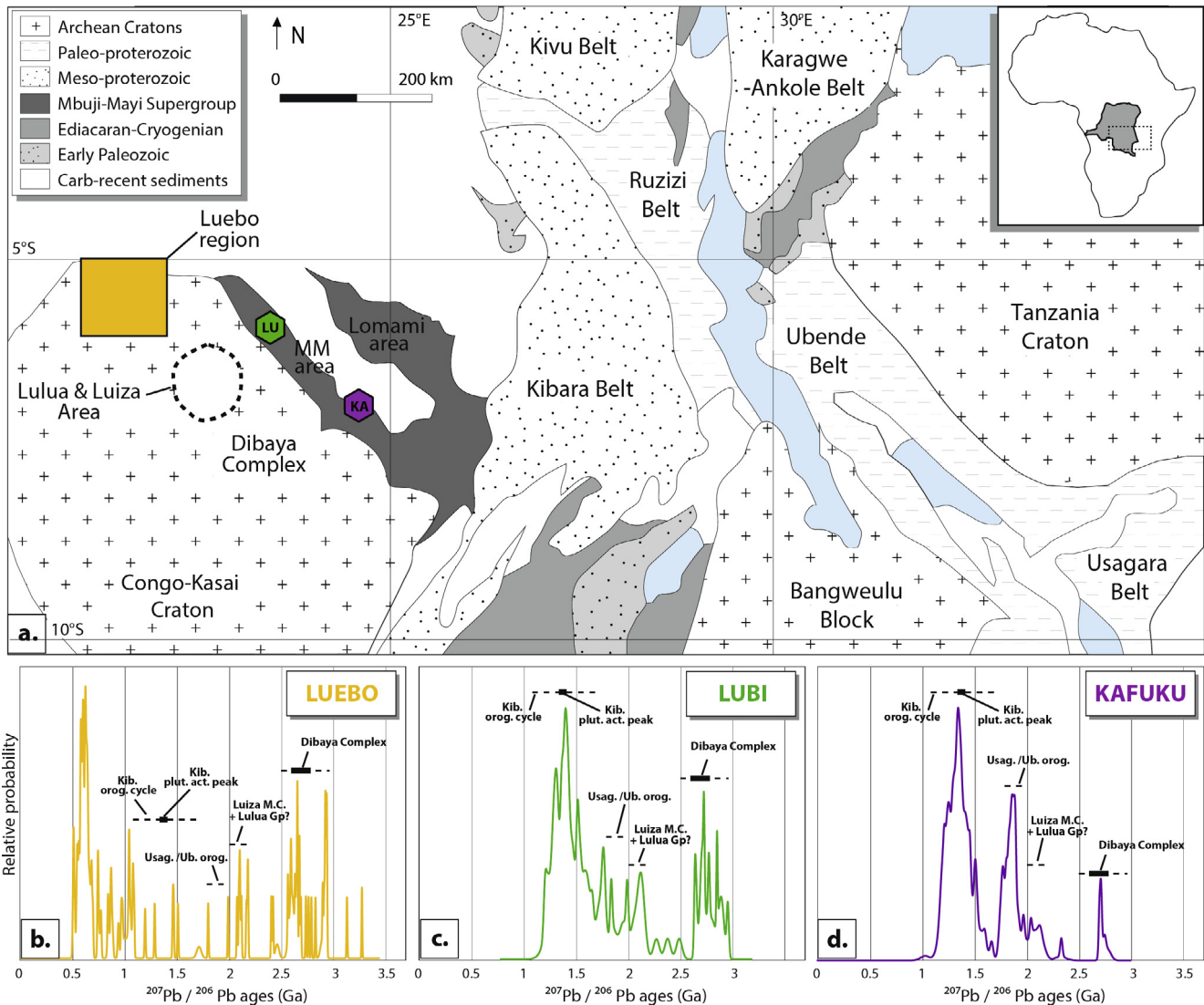
Fig. 10. (a) Geological map of Archean cratons and Proterozoic to Palezoic belts near the study area. Compilation of ^{207}Pb/^{206}Pb apparent ages (Ga) on (b) zircons from the Luebo region (Batumike et al., 2009), (c) xenotimes, monazites and zircons in the Lubi drill core (*this study;* Delpomdor et al., 2013) and (d) xenotimes, monazites and zircons in the Kafuku drill core (*this study;* Delpomdor et al., 2013). Modified after Kadima et al. (2011) and Baludikay et al. (2016a).

evolution. In particular, they document the evolution of biological innovations and patterns of diversification of early eukaryotes (e.g. Butterfield, 2015; Javaux, 2011; Javaux and Knoll, 2016; Knoll, 2014). Eukaryotic cells appeared at least 1.7 Ga ago but their diversification increased around 1.2–0.8 Ga (e.g. Knoll, 1992; Xiao et al., 1997; Butterfield, 2000, 2004; Javaux et al., 2003, 2004; Javaux, 2011; Porter et al., 2003; for an alternative view see Cavalier-Smith, 2002). Baludikay et al. (2016a) recently described an exquisitely preserved assemblage of organic-walled microfossils in the Mbuji-Mayi Supergroup, and documented for the first time the diversification of early eukaryotes in Central Africa, similarly to other worldwide assemblages in the Late Mesoproterozoic–Early Neoproterozoic (e.g. Beghin et al., 2017). Africa in general had a poorly documented Proterozoic microfossil record, but recent studies (Baludikay et al., 2016a; Beghin et al., 2017) reported exquisitely preserved assemblages providing accurate dating of the DRC succession is thus of prime importance to better constrain the patterns of early biosphere evolution in Africa and worldwide.

8. Conclusions

This study provides new time constraints for the diagenesis and sediment sources from the lower part of the Mbuji-Mayi Supergroup. The beginning of the BI Group diagenesis is estimated around 1065 Ma while the end is probably around 1030 Ma. We note variations of deposition regime (carbonated *vs* siliciclastic) and supply of sediments between the different drill cores with diverse terrigenous contributions, coming occasionally from more than 100's km away. This study also contributes to date microfossil levels and to the characterization of their paleoenvironments. Our results are consistent with biostratigraphic data from Baludikay et al. (2016a) supporting the occurrence of worldwide changes around the Mesoproterozoic/Neoproterozoic boundary. We significantly improve the constraints on the timing of early eukaryotes diversification, thereby contributing to a better understanding of early biosphere evolution, preserved in the Democratic Republic of Congo rock record and more broadly in the understudied Proterozoic African deposits.
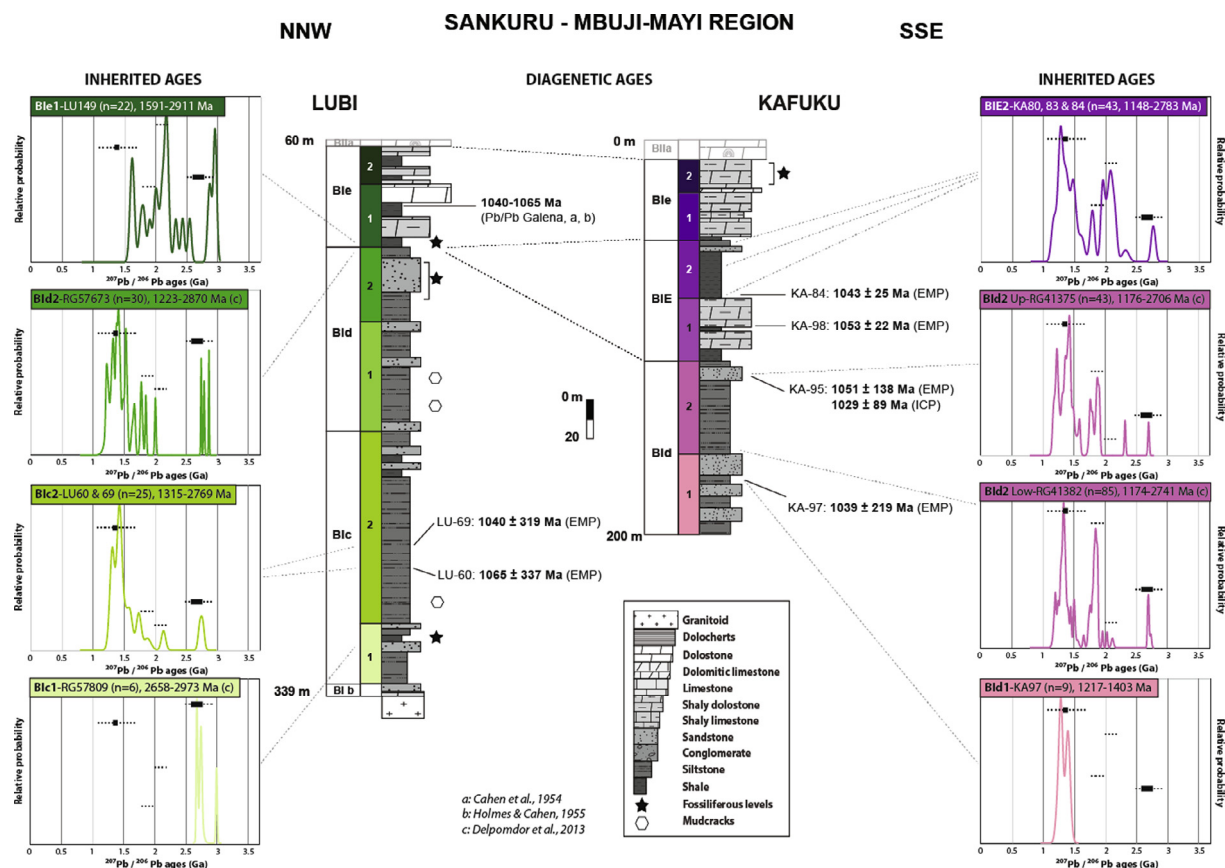
Fig. 11. Sources of inherited ^{207}Pb/^{206}Pb apparent ages (Ga) during the deposition in the Lubi drill core (*this study and* Delpomdor et al., 2013) and in the Kafuku drill core (*this study and* Delpomdor et al., 2013). Diagenetic ages are also shown on the logs. (EMP): Electron MicroProbe; (ICP): ICP-MS. See Fig. 10 for legends. Logs modified after Delpomdor et al. (2013).

Acknowledgements

References

Ancey, M., Bastenaire, F., Tixier, R., 1978. Application des méthodes statistiques en microanalyse. Microanalyse Microscopie électronique à Balayage, 323–347.

Asami, M., Suzuki, K., Grew, E.S., 2002. Chemical Th-U-total Pb dating by electron microprobe analysis of monazite, xenotime and zircon from the Archean Napier Complex, East Antarctica: evidence for ultra-high-temperature metamorphism at 2400 Ma. Precambr. Res. 114 (3), 249–275.

Baludikay, B.K., Storme, J.-Y., François, C., Baudet, D., Javaux, E.J., 2016a. A diverse and exquisitely preserved organic-walled microfossil assemblage from the Meso-Neoproterozoic Mbuji-Mayi Supergroup (Democratic Republic of Congo) and implications for Proterozoic biostratigraphy. Precambr. Res. 281, 166–184.

Baludikay, B.K., Storme, J.-Y., Baudet, D., François, C., Javaux, E., 2016b. Thermal maturation of carbonaceous material from Mbuji-Mayi Supergroup (Kasai, Democratic Republic of Congo). Geophys. Res. Abstr. 18. EGU2016-4574.

Batumike, J.M., Griffin, W.L., O'Reilly, S.Y., Belousova, E.A., Pawlitschek, M., 2009. Crustal evolution in the central congo-kasai craton, luebo, DR congo: insights from zircon U-Pb ages, Hf-isotope and trace-element data. Precambr. Res. 170 (1), 107–115.

Begg, G.C., Griffin, W.L., Natapov, L.M., O'Reilly, S.Y., Grand, S.P., O'Neill, C.J., Hronsky, J.M.A., Poudjom Djomani, Y., Swain, C.J., Deen, T., Bowden, P., 2009. The lithospheric architecture of Africa: seismic tomography, mantle petrology, and tectonic evolution. Geosphere 5 (1), 23–50.

Beghin, J., Storme, J.Y., Houzay, J.P., Blanpied, C., Gueneli, N., Brocks, J.J., Poulton, S.W., Javaux, E.J., 2017. Microfossils from the Late Mesoproterozoic (1.1 Ga) Atar/El Mreïti Groups, Taoudeni Basin, Mauritania, Northwestern Africa. Precambr. Res. 291, 63–82.

Bertrand-Sarfati, J., 1972. Stromatolites columnaires du Précambrien supérieur du Sahara nord-occidental: inventaire, morphologie et microstructure des laminations, corrélations stratigraphiques. Éditions du Centre national de la recherche scientifique.

Bonhomme, M., Clauer, N., 1972. Possibilités d'utilisation stratigraphique des datations directes rubidium-strontium sur les minéraux et les roches sédimentaires. Mém. Bur. Rech. Géol. Min 77, 943–950.

Boven, A., Theunissen, K., Sklyarov, E., Klerkx, J., Melnikov, A., Mruma, A., Punzalan, L., 1999. Timing of exhumation of a high-pressure mafic granulite terrane of the Paleoproterozoic Ubende belt (West Tanzania). Precambr. Res. 93 (1), 119–137.

Butterfield, N.J., 2000. Bangiomorpha pubescens n. gen., n. sp.: implications for the evolution of sex, multicellularity, and the Mesoproterozoic/Neoproterozoic radiation of eukaryotes. Paleobiology 26 (3), 386–404.

Butterfield, N.J., 2004. A vaucheriacean alga from the middle Neoproterozoic of Spitsbergen: implications for the evolution of Proterozoic eukaryotes and the Cambrian explosion. Paleobiology 30 (02), 231–252.

Butterfield, N.J., 2015. Early evolution of the Eukaryota. Palaeontology 58 (1), 5–17.

Cahen, L., 1954. Résultats géochronologiques obtenus sur des minéraux du Congo jusqu'en Mai 1954. Bulletin de La Société Géologique de Belgique 77, B268–B281.

Cahen, L., 1972. L'Ouraninite de 620 ma post-date tout le Katangien, mise au point. Mus. roy. Afr. centr. Dept. Géol. Minér. Rapp. Ann., 35–38

Cahen, L., 1974. Geological background to the copper-bearing strata of southern Shaba (Zaire). Ann. Soc. Géol. Belg., 57–77

Cahen, L., Ledent, D., Snelling, N.J., 1974. Données géochronologiques dans le Katangien inférieur du Kasaï oriental et du Shaba nord-oriental (République du Zaïre). Mus. Roy. Afr. Centr.-Tervuren (Belg.) Dépt. Geol. Min. Rapport Annuel 1974, 51–70.

Cahen, L., Snelling, N.J., Delhal, J., Vail, J.R., Bonhomme, M., Ledent, D., 1984. The Geochronology and Evolution of Africa. Oxford, Clarendon.

Cavalier-Smith, T., 2002. The phagotrophic origin of eukaryotes and phylogenetic classification of Protozoa. Int. J. Syst. Evol. Microbiol. 52 (2), 297–354.

Clauer, N., 1973. Utilisation de la méthode rubidium-strontium pour la datation de niveaux sédimentaires du Précambrien supérieur de l'Adrar mauritanien (Sahara occidental) et la mise en évidence de transformations précoces des minéraux argileux. Geochim. Cosmochim. Acta 37 (10), 2243–2255.

Cocherie, A., Legendre, O., Peucat, J.J., Kouamelan, A.N., 1998. Geochronology of polygenetic monazites constrained by in situ electron microprobe Th-U-total lead determination: implications for lead behaviour in monazite. Geochim. Cosmochim. Acta 62 (14), 2475–2497.

Collins, A.S., Reddy, S.M., Buchan, C., Mruma, A., 2004. Temporal constraints on Palaeoproterozoic eclogite formation and exhumation (Usagaran Orogen, Tanzania). Earth Planet. Sci. Lett. 224 (1), 175–192.

Crowley, J.L., Ghent, E.D., 1999. An electron microprobe study of the U-Th-Pb systematics of metamorphosed monazite: the role of Pb diffusion versus overgrowth and recrystallization. Chem. Geol. 157 (3), 285–302.

De Waele, B., 2004. The Proterozoic Geological History of the IRUMIDE Belt, Zambia Unpublished MSc Thesis. Curtin University of Technology, Australia.

De Waele, B., Fitzsimons, I.C.W., 2007. The nature and timing of Palaeoproterozoic sedimentation at the southeastern margin of Congo Craton; zircon U-Pb geochronology of plutonic, volcanic and clastic units in northern Zambia. Precambr. Res. 159 (1), 95–116.

De Waele, B., Johnson, S.P., Pisarevsky, S.A., 2008. Palaeoproterozoic to Neoproterozoic growth and evolution of the eastern Congo Craton: its role in the Rodinia puzzle. Precambr. Res. 160 (1), 127–141.

Delhal, J. and Ladmirant, H. (1979). Carte géologique à l'échelle du 1/200.000, Notice explicative de la feuille Mbuji-Mayi (Degré carré S7/23) (Service géologique, bureau de Kinshasa).

Delhal, J., Ledent, D., 1973. L'âge du complexe métasédimentaire de Luiza, région du Kasai, Zaïre. Ann. Soc. Géol. Belg. 96, 289–300.

Delhal, J., Ledent, D., Pasteels, P., 1975. L'âge du complexe granitique et migmatitique de Dibaya (Région du Kasaï, Zaïre) par les méthodes Rb-Sr et U-Pb. Ann. Soc. Géol. Belg. 98, 141–154.

Delpomdor, F., 2013. Lithostratigraphie et Sédimentologie De La Chaîne Ouest Congolienne du Néoprotérozoïque Supérieur (Formation de la Diamictite Supérieure et Sous-Groupe du Schisto-Calcaire) Bas-Congo, République Démocratique du Congo Unpublished MSc Thesis. Université Libre de Bruxelles, Belgium.

Delpomdor, F., Linnemann, U., Boven, A., Gärtner, A., Travin, A., Blanpied, C., Preat, A., 2013. Depositional age, provenance, and tectonic and paleoclimatic settings of the late Mesoproterozoic-middle Neoproterozoic Mbuji-Mayi Supergroup, Democratic Republic of Congo. Palaeogeogr. Palaeoclimatol. Palaeoecol. 389, 4–34.

Delpomdor, F., Blanpied, C., Virgone, A., Préat, A., 2015. Sedimentology and sequence stratigraphy of the late precambrian carbonates of the mbuji-mayi supergroup in the sankuru-mbuji-mayi-lomami-lovoy basin (Democratic Republic of the Congo). In: Geology and Resource Potential of the Congo Basin. Springer, pp. 59–76.

Fernandez-Alonso, M., Cutten, H., De Waele, B., Tack, L., Tahon, A., Baudet, D., Barritt, S.D., 2012. The Mesoproterozoic Karagwe-Ankole Belt (formerly the NE Kibara Belt): The result of prolonged extensional intracratonic basin development punctuated by two short-lived far-field compressional events. Precambr. Res. 216, 63–86.

François, C., Kabamba Baludikay, B., Storme, J.-Y., Baudet, D., Paquette, J.-L., Fialin, M., Javaux, E., 2016. New geochronological history of the Mbuji-Mayi Supergroup (Proterozoic, DRC) through U-Pb and Sm-Nd dating. Geophys. Res. Abstr. 18. EGU2016-6405.

Goncalves, P., Nicollet, C., Montel, J.-M., 2004. Petrology and in situ U-Th-Pb monazite geochronology of ultrahigh-temperature metamorphism from the Andriamena mafic unit, north–central Madagascar. Significance of a petrographical P-T path in a polymetamorphic context. J. Petrol. 45 (10), 1923–1957.

Goncalves, P., Williams, M.L., Jercinovic, M.J., 2005. Electron-microprobe age mapping of monazite. Am. Mineral. 90 (4), 578–585.

Griffin, B.J., Forbes, D., McNaughton, N.J., 2000. An evaluation of dating of diagenetic xenotime by electron microprobe. Microsc.Microanal. N. Y. 6 (2), 408–409.

Harrison, T.M., Catlos, E.J., Montel, J.-M., 2002. U-Th-Pb dating of phosphate minerals. Rev. Mineral. Geochem. 48 (1), 524–558.

Holmes, A., Cahen, L., 1955. African geochronology. Colonial Geol. Miner. Resour. 5 (1), 3–38.

Hurai, V., Paquette, J.L., Huraiová, M., Konečný, P., 2010. Age of deep crustal magmatic chambers in the intra-Carpathian back-arc basin inferred from LA-ICPMS U-Th-Pb dating of zircon and monazite from igneous xenoliths in alkali basalts. J. Volc. Geo. Res. 198, 275–287.

Jackson, S.E., Pearson, N.J., Griffin, W.L., Belousova, E.A., 2004. The application of laser ablation-inductively coupled plasma-mass spectrometry to in situ U-Pb zircon geochronology. Chem. Geol. 211 (1), 47–69.

Javaux, E. (2011). Early eukaryotes in Precambrian oceans. *Origins and Evolution of Life: An Astrobiological Perspective*, 414–449.

Javaux, E.J., Knoll, A.H., 2016. Micropaleontology of the lower Mesoproterozoic Roper Group, Australia and implications for early eukaryote evolution. J. Paleontol. 91 (2), 199–229.

Javaux, E.J., Knoll, A.H., Walter, M., 2003. Recognizing and interpreting the fossils of early eukaryotes. Orig. Life Evol. Biosph. 33 (1), 75–94.

Javaux, E.J., Knoll, A.H., Walter, M.R., 2004. TEM evidence for eukaryotic diversity in mid-Proterozoic oceans. Geobiology 2 (3), 121–132.

Jercinovic, M.J., Williams, M.L., 2005. Analytical perils (and progress) in electron microprobe trace element analysis applied to geochronology: Background acquisition, interferences, and beam irradiation effects. Am. Mineral. 90 (4), 526–546.

Johnson, S.P., Rivers, T., De Waele, B., 2005. A review of the Mesoproterozoic to early Palaeozoic magmatic and tectonothermal history of south–central Africa: implications for Rodinia and Gondwana. J. Geol. Soc. 162 (3), 433–450.

Kadima, E., Delvaux, D., Sebagenzi, S.N., Tack, L., Kabeya, S.M., 2011. Structure and geological history of the Congo Basin: an integrated interpretation of gravity, magnetic and reflection seismic data. Basin Res. 23 (5), 499–527.

Knoll, A.H., 1992. The early evolution of eukaryotes: a geological perspective. Science 256 (5057), 622.

Knoll, A.H., 2014. Paleobiological perspectives on early eukaryotic evolution. Cold Spring Harbor Perspect. Biol. 6 (1), a016121.

Kokonyangi, J., Armstrong, R., Kampunzu, A.B., Yoshida, M., Okudaira, T., 2004. U-Pb zircon geochronology and petrology of granitoids from Mitwaba (Katanga, Congo): implications for the evolution of the Mesoproterozoic Kibaran belt. Precambr. Res. 132 (1), 79–106.

Kokonyangi, J.W., Kampunzu, A.B., Armstrong, R., Yoshida, M., Okudaira, T., Arima, M., Ngulube, D.A., 2006. The mesoproterozoic kibaride belt (Katanga, SE DR Congo). J. Afr. Earth Sc. 46 (1), 1–35.

Kokonyangi, J.W., Kampunzu, A.B., Armstrong, R., Arima, M., Yoshida, M., Okudaira, T., 2007. U-Pb SHRIMP dating of detrital zircons from the Nzilo group (Kibaran Belt): implications for the source of sediments and mesoproterozoic evolution of Central Africa. J. Geol. 115 (1), 99–113.

Lenoir, J.L., Liégeois, J.-P., Theunissen, K., Klerkx, J., 1994. The Palaeoproterozoic Ubendian shear belt in Tanzania: geochronology and structure. J. Afr. Earth Sc. 19 (3), 169–184.

Ludwig, K.L., 2001. Using Isoplot/EX, v2. 49, a Geochronological Toolkit for Microsoft Excel. Geochronological Center Special Publication, Berkeley.

McNaughton, N.J., Rasmussen, B., Fletcher, I.R., 1999. SHRIMP uranium-lead dating of diagenetic xenotime in siliciclastic sedimentary rocks. Science 285 (5424), 78–80.

Möller, A., Appel, P., Mezger, K., Schenk, V., 1995. Evidence for a 2 Ga subduction zone: eclogites in the Usagaran belt of Tanzania. Geology 23 (12), 1067–1070.

Montel, J.M., Veschambre, M., Nicollet, C., 1994. Datation de la monazite à la microsonde électronique. Comptes rendus de l'Académie des sciences. Série 2. Sciences de la terre et des planètes 318 (11), 1489–1495.

Montel, J.-M., Foret, S., Veschambre, M., Nicollet, C., Provost, A., 1996. Electron microprobe dating of monazite. Chem. Geol. 131 (1), 37–53.

Montel, J.M., Kornprobst, J., Vielzeuf, D., 2000. Preservation of old U-Th-Pb ages in shielded monazite: example from the Beni Bousera Hercynian kinzigites (Morocco). J. Metamorph. Geol. 18 (3), 335–342.

Paquette, J.-L., Tiepolo, M., 2007. High resolution (5 μm) U-Th-Pb isotope dating of monazite with excimer laser ablation (ELA)-ICPMS. Chem. Geol. 240 (3), 222–237.

Paquette, J.L., Piro, J.L., Devidal, J.L., Bosse, V., Didier, A., 2014. Sensitivity enhancement in LA-ICP-MS by N2 addition to carrier gas: application to radiometric dating of U-Th-bearing minerals. Agilent ICP-MS J. 58, 4–5.

Parrish, R.R., 1990. U-Pb dating of monazite and its application to geological problems. Can. J. Earth Sci. 27 (11), 1431–1450.

Porter, S.M., Meisterfeld, R., Knoll, A.H., 2003. Vase-shaped microfossils from the Neoproterozoic Chuar Group, Grand Canyon: a classification guided by modern testate amoebae. J. Paleontol. 77 (03), 409–429.

Rasmussen, B., Muhling, J.R., 2007. Monazite begets monazite: evidence for dissolution of detrital monazite and reprecipitation of syntectonic monazite during low-grade regional metamorphism. Contrib. Mineral. Petrol. 154 (6), 675–689.

Raucq, P., 1957. Contribution à la connaissance du Système de la Bushimay. Annales Du Musée Royal Du Congo Belge (Tervuren) 8 (18), 427.

Raucq, P., 1970. Nouvelles acquisitions sur le systeme de la Bushimay. Annales/ Musee de l'Afrique Centrale. Sciences Geologiques 8 (69).

Reddy, S.M., Collins, A.S., Mruma, A., 2003. Complex high-strain deformation in the Usagaran Orogen, Tanzania: structural setting of Palaeoproterozoic eclogites. Tectonophysics 375 (1), 101–123.

Shaw, C.A., Karlstrom, K.E., Williams, M.L., Jercinovic, M.J., McCoy, A.M., 2001. Electron-microprobe monazite dating of ca. 1.71-1.63 Ga and ca. 1.45-1.38 Ga deformation in the Homestake shear zone, Colorado: Origin and early evolution of a persistent intracontinental tectonic zone. Geology 29 (8), 739–742.

Sommer, H., Kröner, A., Muhongo, S., Hauzenberger, C., 2005. SHRIMP zircon ages for post-Usagaran granitoid and rhyolitic rocks from the Palaeoproterozoic terrain of southwestern Tanzania. S. Afr. J. Geol. 108 (2), 247–256.

Suzuki, K., Adachi, M., 1991. Precambrian provenance and Silurian metamorphism of the Tsubonosawa paragneiss in the South Kitakami terrane, Northeast Japan, revealed by the chemical Th-U-total Pb isochron ages of monazite, zircon and xenotime. Geochem. J. 25 (5), 357–376.

Suzuki, K., Adachi, M., 1994. Middle Precambrian detrital monazite and zircon from the Hida gneiss on Oki-Dogo Island, Japan: their origin and implications for the correlation of basement gneiss of Southwest Japan and Korea. Tectonophysics 235 (3), 277–292.

Tack, L., Baudet, D., Chartry, G., Deblond, A., Fernandez-Alonso, M., Lavreau, J., others. (2002). The Northeastern Kibaran Belt (NKB) reconsidered: evidence for a c. 1370 Ma-old, repeatedly reactivated Kibara mobile belt, preceding the c. 1.0

Ga Rodinia Supercontinent assembly. in: 19th Colloquium of African Geology, El Jadida, Morocco (pp. 19–23).

Tack, L., Wingate, M.T.D., De Waele, B., Meert, J., Belousova, E., Griffin, B., Fernandez-Alonso, M., 2010. The 1375Ma "Kibaran event" in Central Africa: Prominent emplacement of bimodal magmatism under extensional regime. Precambr. Res. 180 (1), 63–84.

Terry, M.P., Robinson, P., Hamilton, A., Jercinovic, M.J., 2000. Monazite geochronology of UHP and HP metamorphism, deformation, and exhumation, Nordøyane, Western Gneiss Region, Norway. Am. Mineral. 85 (11–12), 1651–1664.

Tomascak, P.B., Krogstad, E.J., Walker, R.J., 1996. U-Pb monazite geochronology of granitic rocks from Maine: implications for late Paleozoic tectonics in the northern Appalachians. J. Geol. 104 (2), 185–195.

Van Achterbergh, E., Ryan, C. G., Jackson, S. E., Griffin, W. L. (2001). Data reduction software for LA-ICP-MS. Laser-Ablation-ICPMS in the Earth Sciences—principles and Applications. Miner Assoc Can (short Course Series), 29, 239–243.

Wazilewski, I., 1953. Exploration En Profondeur Des Formations Du Système De La Bushimay (Bakwanga. Université de Louvain, Kasai, Congo Belge.

Williams, M.L., Jercinovic, M.J., 2002. Microprobe monazite geochronology: putting absolute time into microstructural analysis. J. Struct. Geol. 24 (6), 1013–1028.

Williams, M.L., Jercinovic, M.J., Terry, M.P., 1999. Age mapping and dating of monazite on the electron microprobe: Deconvoluting multistage tectonic histories. Geology 27 (11), 1023–1026.

Xiao, S., Knoll, A.H., Kaufman, A.J., Yin, L., Zhang, Y., 1997. Neoproterozoic fossils in Mesoproterozoic rocks? Chemostratigraphic resolution of a biostratigraphic conundrum from the North China Platform. Precambr. Res. 84 (3), 197–220.